Astron. Astrophys. 287, 990–1013 (1994)

ASTRONOMY
AND
ASTROPHYSICS

Meteor stream activity

I. The annual streams*

P. Jenniskens[1,2]

[1] Dutch Meteor Society, Lederkarper 4, NL-2318 NB Leiden, The Netherlands
[2] NASA/Ames Research Center, Mail Stop 239-4, Moffett Field, CA 94035-1000, USA

Received 31 August 1993 / Accepted 8 December 1993

Abstract. Between 1981 and 1991, a small group of amateur meteor observers in Australia and the Netherlands counted meteors during 4,482 hours of effective observing time. These counts have been reduced and are to be presented here as a first homogeneous set of some 50 meteor stream activity curves for all major and many minor meteor streams on both hemispheres. Together with the sporadic background, these give an accurate picture of annual meteor activity.

Empirical corrections are given that relate the observed meteor rates to well defined Zenith Hourly Rates (ZHR).

It is found that all major streams are well represented by a set of exponential curves: $ZHR = ZHR_{max} 10^{-B|\lambda_\odot - \lambda_\odot^{max}|}$. Values of ZHR_{max} and B are given. There is no evidence for stable sub-maxima in the activity profiles. In four, and possibly six, cases, there is evidence for a background component in the activity curve. In all cases, the background is more extended to small solar longitude $\lambda_\odot$.

From a fit of the above dependence to the rates of minor streams, it is found that the slopes of most high inclination (i> 15°) streams have a characteristic value of B = 0.19±0.08 per degree of solar longitude increase in the ^{10}log of the ZHR.

The ZHR is transformed into mass influx rates, from which the total mass in the meteoroid stream is estimated by making an assumption about the distribution of matter perpendicular to the path of the Earth. Total masses of the observed streams are of order 10^{14} to 10^{16}g.

Key words: meteors: meteoroids – comets: general

1. Introduction

A significant part of meteor activity is associated with meteor streams: meteoroids that enter the Earth's atmosphere at similar entry velocity and at nearly parallel trajectories, which cause the meteors to radiate from a virtual point on the sky that is called the radiant. These meteoroids have a common origin, usually - if not always - they are the debris from the decay of, sometimes extinct, short-period comets (e.g. Hughes 1978; Lindblad 1980; McIntosh 1991).

The annual streams are those streams that occur every year, over a period of days, when the Earth passes the orbit of the parent comet. The meteor rates vary as a function of the Earth's position in its orbit, increasing to a peak and decreasing. The shape of this, which is called the activity curve, reflects both the cometary dust ejection process and the subsequent orbital evolution of meteoroids after ejection from the comet. Computing techniques have developed to a point where meteor stream evolution can be studied theoretically, but the interpretation of the simulations is hampered by a lack of observational data (e.g. Hughes et al. 1979; Williams et al. 1979; Murray et al. 1980; Fox et al. 1982; Jones 1985; McIntosh & Jones 1988; McIntosh 1991).

Radar observations are potentially a powerful tool to obtain data on meteor rates but there is a major difficulty in discriminating between stream members and others (the sporadic meteors) and in correcting the observed raw data to meteor influx. Activity curves have been derived of the major meteor streams, i.e. of the Perseids (Kaiser et al. 1966; Lindblad & Simek 1986; Simek & Lindblad 1990), the Orionids (Webster et al. 1966; Jones 1983), the Lyrids (Porubcan 1986), the Geminids (Poole et al. 1972; McIntosh & Simek 1980), and the Bootids (McIntosh & Simek 1984; Bel'kovich et al. 1984). TV image intensifiers (Image Photon Counting Systems) potentially do allow a more accurate stream member classification, but the meteor streams are not easily detected in the smaller mass range covered by the current systems. No activity curves have been published yet.

Visual (naked eye) observers are able to detect an order of magnitude lower stream rates than current radar observa-

Send offprint requests to: NASA/Ames Research Center (peter@ax.arc.nasa.gov).

* Tables 3a-c are also available in electronic form: see the editorial in A&A 1993, Vol. 280 No 3, page E1;
Part of this work was done while at Leiden Observatory.

tions due to an easier discrimination between stream members and sporadic meteors. Meteors have been counted by visual observers since the first half of the 19th century (Hughes 1982) and many of these counts have been gathered and published over the years, notably by W.F. Denning (Journal of the B.A.A.), C.P. Olivier (Popular Astronomy) and P.M. Millman (J.R.A.S. Canada). These early data are usually not corrected for atmospheric conditions, observer's perception or even radiant altitude dilution. The first few reliable rate profiles were published only recently by a number of amateur meteor observers and by V. Porubcan et al. from a series of observations obtained at Skalnaté Pleso Observatory between 1944-1953 (BAC, Contr. Astr. Obs. Skalnaté Pleso).

The gathering of meteor counts by amateur observers has gained a big momentum in the past fifteen years. Many activity curves of single returns have been published by a.o. R. Veltman (Radiant, the Journal of the Dutch Meteor Society), J. Wood (NAPO-MS Bulletins), G.A. Spalding (Journal of the B.A.A.), and recently notably by R. Koschack, P. Roggemans, and J. Rendtel (WGN, the Journal of the International Meteor Organisation).

Attempts to improve statistics by combining data from several independent groups have led to the recognition of common systematic errors in the data amounting to factors of two or more (Millman 1967; Spalding 1987). Individual counts are usually of low accuracy due to instrumental variations (that is, observer perception), subjective estimates of the sky condition, and low detection rates of about 10 meteors per hour typically.

This paper attempts to derive a homogeneous set of activity curves by combining the counts of experienced observers in a limited number of independent groups, that is, one on each hemisphere. The counts have been obtained in the eleven years from 1981 to 1991. The paper is ordered as follows: Sect. 2 describes the observing technique and data selection; Sect. 3 discusses the correction factors for sky condition, observer perception, and radiant altitude dilution; Sect. 4 and Sect. 5 present results in terms of zenith hourly rates; and in Sect. 6 the zenith hourly rates are transformed into mass influx rates and from that the total mass of matter in the meteoroid stream is estimated.

2. Observations

The meteor counts selected for this project amount to 110,538 meteors recorded in 4,482 hours of net observing time by 10 observers of the Dutch Meteor Society (DMS) and 6 observers of the North Australian Planetary Observers – Meteor Section (NAPO–MS). Raw data of the latter group are published by Jeff Wood in the W.A.M.S. Bulletins and, since 1986, in the N.A.P.O.–M.S. Bulletins. DMS raw data are gathered from the visual archive compiled by Rudolf Veltman and the author from which preliminary results have been published in Radiant. The selected observers are the 10 most productive observers of DMS before 1988 and those observers of NAPO-MS who were active for a period of at least three consecutive years.

Table 1. Observer statistics. Location: S = southern hemisphere (North Australian Planetary Observers - Meteor Section), N = northern hemisphere (Dutch Meteor Society). c_p: average sporadic hourly rate normalised to 10. ϵ: parameter that describes the limiting magnitude scale (Eq. 3). T_{eff}: effective observing time in hours. N: number of observed meteors

Observer	Loc.	$c_p \pm \sigma c_p$	ϵ	T_{eff}	$N_{meteors}$
Jeff Wood	S	1.81 ±0.13	0.57	1,152	36,557
Darren Ferdinandez	S	1.31 0.17	0.51	629	10,405
Koen Miskotte	N	1.24 0.09	0.79	393	10,760
Klaas Jobse	N	1.25 0.10	0.70	390	10,134
Bauke Rispens	N	1.14 0.14	0.75	272	7,592
Nicolas Harvey	S	2.28 0.21	0.61	230	9,437
Peter Jenniskens	N	0.80 0.07	0.63	213	3,448
Marc de Lignie	N	0.98 0.05	0.87	199	4,848
Hans Breukers	N	0.66 0.03	0.50	193	2,996
George Platt	S	1.09 0.05	0.57	172	4,080
Rudolf Veltman	N	0.95 0.06	0.67	166	2,225
Jos Nijland	N	0.66 0.03	0.68	107	2,282
Jeff Malone	S	1.02 0.03	0.81	105	1,739
Hans Betlem	N	0.63 0.05	0.43	100	1,512
David Cake	S	1.02 0.04	0.59	97	1,869
Joop Bruining	N	0.94 0.04	0.70	64	654
total: 16 obs.				4,482	110,538

2.1. *Observing technique and data selection*

Meteors are counted by naked eye, while the observer sits comfortably in a chair, or lays on a reclining lawn chair, and leisurely scans the sky (e.g. Jenniskens 1988; Bone 1993). The observer keeps the center of vision between 20 and 60 degrees from the active radiant and at altitudes of 60-90 degrees above the horizon. The observer's feet usually point within 90 degrees from the radiant. The field of view has less than 20% obstruction. An estimate of the sky limiting magnitude (Lm) is made by counting stars in predesigned areas. Values range between Lm = 5.2 and 7.2. Data with limiting magnitudes less than 5.2 are omitted from the sample. Dead time for recording is restricted to less than 20% and observing intervals should exceed an effective observing time T_{eff} = 0.4 hours.

The individual meteors are recorded using either gnomonic starmaps and observing forms or tape recorders. The difference in technique concerns the possible errors in classification. Gnomonic starmaps allow meteor classification at a later time, using criteria that are more homogeneous for all observers. Classification is based on meteor direction (allowing for radiant drift), angular velocity, and the length of the meteor trails on the sky with respect to the angular distance from the radiant. Data logged on gnomonic starmaps are used for the minor streams and the tails of the major streams. Meteors logged on a tape recorder are used for the cores of the major streams, unless the observers were well aware of the radiant position.

The database contains numerous zero detections, that is, observing periods in which no stream members are detected. This is a not a trivial point. Zero detections are often neglected, because it is not always clear whether an observer paid attention to

a particular minor stream. Negligence leads to an overestimation of rates of minor streams in the wings while unjustified inclusion of zero detections results in an artifical decrease of activity. I chose to include such zero detections only when the stream is mentioned during other hours of the night, or at some moment in the same campaign of several nights. Of course, this problem does not exist when data are logged on gnomonic starmaps.

The number of streams to be studied has been limited to approximately 50 in order to obtain a well defined sporadic background rate; sporadic meaning any meteor that does not belong to one of the selected streams. The sporadic rate in certain seasons of the year will be used to normalise stream rates in order to account for a variable observer perception. For this purpose it is neccesary to exclude the same minor streams from the sporadic rates in all observations. The northern hemisphere streams are a selection of those listed by Lindblad (1971) and Cook (1973), from photographic surveys of orbital elements, while the selection of southern hemisphere streams is based on the streams classified by experienced observer Jeff Wood. Other minor streams are known to be active, but have given too few data to allow the construction of an activity curve, f.e. η Lyrids (Iras-Araki-Alcockids) on May 10th and Pegasids on July 10th.

Even on the northern hemisphere, photographic surveys may, occasionally, have missed a minor stream. Indeed, in the cause of the reduction of northern hemisphere data from archived starmaps I found one, only one, such minor stream not previously mentioned that might warrant further investigation: 72 medium fast meteors were observed to radiate apparently from RA = 304, DEC = +48 in a few days around July 17-22. Following this find, a watch in 1990 gave a radiant at RA,DEC = 300,+52 (15 meteors, Jenniskens et al. 1991) and a watch by the author in 1993 resulted again in RA,DEC = 304,+48 (4 meteors). Photographic confirmation is weak: one possible member was photographed in Dushanbe on 1961 July 12: RA = 304.5, DEC = +49.7, V_∞ = 41.0 km/s (Babadzhanov & Kramer 1965). The o Cygnids are added to the selection of streams, but these observations need further confirmation before it can be excluded that they are merely due to a chance alignment of sporadic meteors or meteors of other minor streams, for example, the o Draconids listed in Cook (1973) ($\lambda_\odot$ = 1·12; RA,DEC = 271,+59; V_∞ = 24 km/s).

Note that a photographic survey is lacking for the southern hemisphere and the recognition of meteor streams depends, to a large extend, on visual observations. Limited radar data are available but only, with a few exceptions, for weak and relatively slow meteors (Nilsson 1964; Gatrell & Elford 1975). The meteor streams detected in these radar surveys show little overlap with the streams that are recognised visually (and photographically), similar to northern hemisphere radar surveys. Consequently, for some of the mentioned southern hemisphere minor 'streams' it needs to be proven that the meteoroids move in similar orbits, notably for the δ Velids, the α Crucids, the θ Centaurids, the Corona Australids, the τ Cetids, the γ Dorids, and δ Eridanids.

Table 3 summarizes the radiant position and drift, the entry velocity, and magnitude distribution index of each of the 50 selected streams. The table also contains the total number of observed meteors of each stream, the total effective observing time and the number of observers that contributed to the data. The total contribution of each individual observer is summarized in Table 1.

3. Normalisation of the counts

Meteor rates are commonly expressed in terms of Zenith Hourly Rates (ZHR), which is the hourly rate of meteors seen by a standard observer in optimum conditions: the radiant in the zenith and a star limiting magnitude of 6.5. The subsequent conversion to mass influx rate contains a number of additional corrections, e.g. the mass of a zero magnitude meteor and the effective surface area monitored. These corrections, however, do not change much with the position of the Earth in its orbit and the ZHR activity profile gives a fair picture of the mass influx profile. For the purpose of knowing how many meteors are to be seen at a given time and under given conditions, the Zenith Hourly Rate is a more convenient unit.

The corrected Zenith Hourly Rate (ZHR) is given by:

$$ZHR = \frac{N}{T_{eff}} \times r^{6.5-Lm} \times sin(h_r)^{-\gamma} \times c_p \qquad (1)$$

where N is the number of stream meteors observed in a time interval T_{eff}, r and γ are stream (and $\lambda_\odot$) dependent constants that describe the corrections for the variables limiting magnitude (Lm) and radiant altitude (h_r) respectively. c_p is an observer dependent perception correction. In this section, each of the three corrections in Eq. 1 will be discussed in some detail.

3.1. The Limiting magnitude correction

The meteor rate is a sensitive function of sky conditions: if few stars are visible, few meteors are seen. Figure 1 shows that the dependence of observed (sporadic) rates on star limiting magnitude (Lm) is exponential, ZHR$\sim r^{6.5-Lm}$. Such an exponential dependence is expected if the detection probability of a meteor of magnitude x at limiting magnitude Lm equals that of a meteor of magnitude $x - 1$ at limiting magnitude Lm -1 (i.e. Van der Veen 1986a,b; Spalding 1987). In that case, the exponent (r) is expected to be equal to the magnitude distribution index (χ):

$$\chi = n(m + 1)/n(m) \qquad (2)$$

where n(m) is the number of observed meteors N(m) of brightness m in a given part of the sky corrected for the detection probability P(m) of such meteors in that part of the sky: n(m) = N(m)/P(m). The detection probability (or "probability function") is discussed in the Appendix. In practice, χ is derived from the magnitude distribution after correction for an assumed probability function or, alternatively, from the ratio of stream and sporadic meteors as a function of magnitude, assuming that the probability function is the same for both and by adopting χ = 3.4 for sporadic meteors (Kresakova 1966). The values reported in Table 3 are a compilation of such studies published in NAPO-MS Bulletin and Radiant.

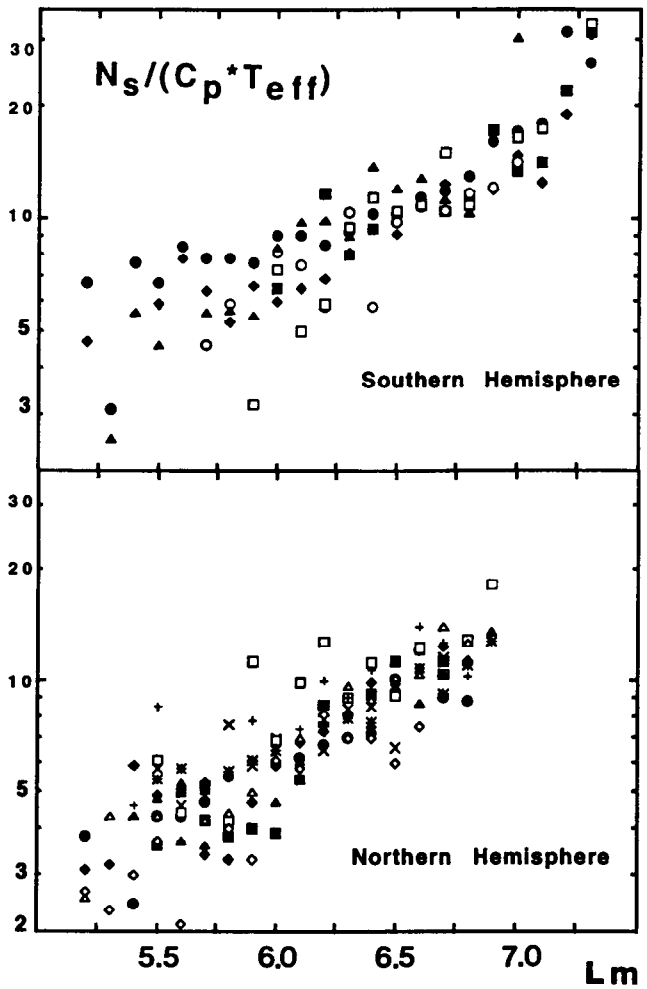

Fig. 1. The limiting-magnitude correction. Sporadic hourly rates, corrected for observer perception (c_p) only, are plotted against the brightness of the faintest star that was seen in a small starfield (Lm). Individual observers are assigned a different symbol

Koschack & Rendtel (1990a,b) argue that r = χ applies for a group of observers of AKM (Germany). However, I find r to be somewhat smaller than χ, possibly because r is also a sensitive function of the limiting magnitude scale, that is, the relationship between star count and sky conditions, which depends somewhat on the observer's judgement. Linear least squares fits to data as in Fig. 1 result in values of r listed in Table 2. These values are compared to χ from Kresakova (1966) and Levin (1955).

Although r seems to be proportional to χ, there is a systematic difference which should be accounted for. Because my main concern is to normalise all counts to a uniform system, I introduce an exponent ϵ, where:

$$r = \chi^{\epsilon} \tag{3}$$

ϵ is observer dependent and reflects individual differences in the limiting magnitude scale. Note that differences in the normalisation point (Lm = 6.5) will be incorporated in the observer's perception coefficient (Sect. 3.4). Values of ϵ are listed in Table 1 and range between 0.43 and 0.87.

A constant value of χ is assumed, both as a function of magnitude in the range m = -3 to +5 (and corresponding mass range of the meteoroids) and as a function of the position along the Earth's path through the stream. The variation of χ is expected to be small over the magnitude range covered. Only for the Bootids and Geminids there is some evidence of a gradual change of χ with magnitude from radar observations (Simek 1987b). However, note that Kresakova (1966) does not see the effect clearly in visual data of the Geminids. All other major streams show linear slopes in the logarithm of the ratio of stream and sporadic meteors versus magnitude between -3 and +5.

For most major streams, the variation of χ along the Earth's path is observed to be small, to the point of being negligible, e.g. for the Perseids (Kaiser et al. 1966; Veltman 1983a; Roggemans 1987; Jenniskens 1989b; Andreev 1989), Orionids (Veltman 1986a; Znojil et al. 1987), and Lyrids (Veltman 1985). There is some indication that χ increases towards the outer edges of these streams, but the data are too uncertain to be of value. On the other hand, significant variations of χ are found, again, for the Bootids and Geminids (Boo: Poole et al. 1972; Simek 1975; Bel'kovich et al. 1984; Van der Veen 1989; Gem: Spalding 1982; Roggemans & Koschack 1991; Jenniskens 1992a; Rendtel et al. 1993a). These variations are well studied and are therefore taken into account. Unfortunately, no such information exists of other (minor) short period streams. Note that the Bootids and Geminids are the two narrowest streams encountered in this study, with the doubtful exception of the Ursids, and their behavior of χ is probably atypical.

For the range of limiting magnitude Lm = 5.2 until 7.2, a characteristic error of $\pm$0.3 in r leads to at most a 15% error in individual rate estimates.

3.2. Correction for moonlight

The moon causes an increase of the brightness of the sky background, which makes meteors and stars more difficult to see. From observations of meteors during the moon eclipses of Jan. 9/10 1982 and May 4/5 1985, Wood (1982b, 1986) found that the decrease of number of meteors observed is exponential with limiting magnitude, with r = 2.6 for sporadic meteors and r = 2.4 for the Eta Aquarids (compared to χ = 3.4 and 2.7 resp.). Again, the r-values are a bit less than the magnitude distribution index suggesting ϵ = 0.78 and 0.88 respectively. Because these data were obtained by other observers than listed in Table 1, and the values of ϵ are in the range of typical values, I conclude that the limiting magnitude correction gives an appropriate correction for sky condition affected by moonlight. In order not to stress this conclusion too much, I included data only for a moon at altitudes of no more than 30 degrees above the horizon, while the limit for phases of 0.7-1.3 around full moon was set to 5 degrees only. The brightness (I) of the moon, and its disturbing influence, peaks sharply near full moon and changes with phase (F) according to: F = 1.0, I = 100%; 0.9, 60%; 0.8, 40%; 0.7, 24%; 0.6, 16%; 0.5, 8%; 0.4, 4%, and 0.3, 2% (Katz 1987). A

Table 2. The limiting magnitude exponent r and the radiant altitude exponent γ as derived by comparing the observed activity in the core of the stream with the activity expected for r = χ and γ = 1.0. [1]: χ by Kresakova (1966) [2]: χ by Levin (1955)

stream		log r	r	χ	[1]	[2]	V_∞	γ	$\gamma_{the.}$
SPO	N	0.37±0.03	2.2-2.5	3.4	3.4	3.0	-	-	-
"	S	0.35±0.04	2.0-2.5	"	"	"	"	-	-
LEO	N	0.56±0.12	2.8-4.8	3.4	2.5	2.4	71	1.23±0.50	1.55
DAZ	N	-	-	3.3	2.7	3.7	43	1.03±0.10	1.48
"	S	0.55±0.12	2.7-4.7	"	"	"	"	-	1.55
ORI	N	0.30±0.20	1.3-3.2	3.1	2.9	4.0	67	1.68±0.14	1.47
"	S	0.42±0.03	2.5-2.8	"	"	"	"	1.60±0.27	1.47
EAQ	S	0.38±0.06	2.1-2.8	2.7	2.3	2.3	66	1.06±0.12	1.45
LYR	N	0.38±0.07	2.0-2.8	2.7	2.9	>1.7	49	1.50±0.50	1.4 3
GEM	N	0.20±0.06	1.4-1.8	2.6	2.6	3.4	36	1.33±0.12	1.40
"	S	0.46±0.08	2.4-3.5	"	"	"	"	1.67±0.32	1.36
PER	N	0.33±0.04	1.9-2.3	2.5	2.4	2.5	61	1.42±0.08	1.41
BOO	N	0.64±0.22	2.6-7.2	2.5	-	2.5	43	1.18±0.08	1.37
TAU	N	0.52±0.10	2.6-4.2	2.3	-	3.0	30	1.67±0.22	1.30
"	S			"	"	"	"	1.60±0.27	1.30
ACE	S	0.03±0.25	0.6-1.9	2.3	-	-	57	1.32±0.18	1.37
CAP	N	0.26±0.14	1.3-2.5	2.0	-	-	25	1.06±0.19	1.13
"	S	0.49±0.04	2.8-3.4	"	"	"	"	1.86±0.28	1.20

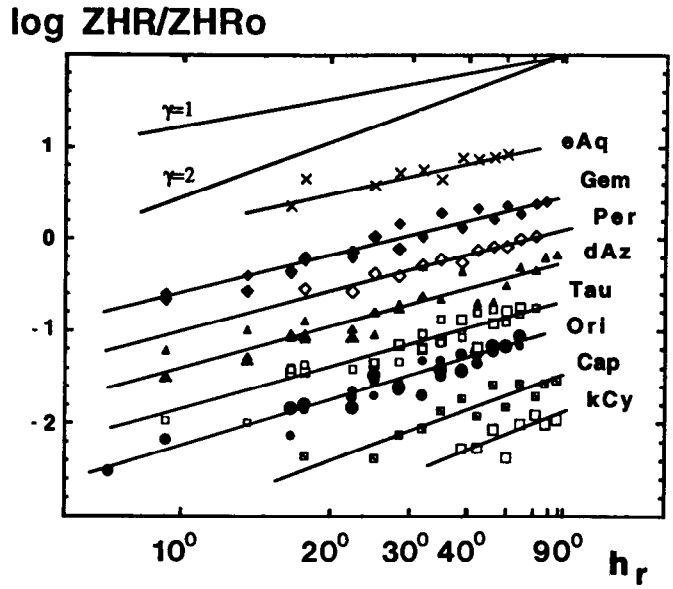

Fig. 2. Radiant altitude correction. The observed rate before radiant altitude (h_r) correction (= ZHR) is compared with rates derived from a fit to data calculated with an assumed γ=1.0 (ZHR_o). The ratio ZHR/ZHR_o is plotted versus $sin(h_r)$ in a log-log diagram. The slope in each graph is approximately equal to the correct γ

nice way of estimating the moon's brightness is given by Knöfel (1990).

3.3. The radiant altitude correction

Radiant altitudes (h_r) of less than 90° dilute the meteor influx per unit area according to approximately: $sin(h_r)^{-1}$. Several authors have suggested extending this correction by including such effects as the finite length of meteor trails: $sin(h_r + 6^o)^{-1}$ (Prentice 1953), the fainter brightness of meteors due to a different gradient of atmospheric density along the path and the increase of meteor trail length $[\gamma' sinh_r + (1 - \gamma')sin^2 h_r]^{-1}$ (Opik 1940, 1958), and the zenith attraction (Kresak 1964):

$$sin(h_r) < \gamma'' + (1 - \gamma'')sin(h_r) \quad (4)$$

where γ'' depends on entry velocity: $\gamma'' = 61.8/V_\infty^2$ in good approximation.

Zvolankova (1983) suggested the general form of Eq. 1, $ZHR \sim sin(h_r)^{-\gamma}$, and derived γ = 1.47±0.11 (1σ) for the Perseid stream. This analysis has been repeated here for several major streams. Figure 2 compares the observed rates before radiant altitude correction (ZHR) with rates derived from a fit to data calculated with γ = 1.0 and r = χ (ZHR_o) and plots the ratio ZHR/ZHR_o as a function of sin (h_r) in a log-log plot. The slope in these plots is close to the actual value of γ. An itterative process does not significantly change this value. γ varies significantly between 1.0 and 1.8, but is typically about 1.4, which is in good agreement with Zvolankova (1983). The value is larger than 1.0, which probably reflects the fainter brightness of meteoids of given mass and entry velocity at lower entry angles. There is no strong dependence on entry velocity, nor on magnitude distribution index. However, γ is expected to depend weakly on χ. In case the fainter meteors (Δm) cause a decrease in number density proportional to $\chi^{\Delta m}$ and Δm relates to h_r according to: $m_{ph} \sim -0.67 log(sin(h_r))$ (Jacchia et al. 1967, from photographic data), one has:

$$\gamma = 1 + 1.08\ log(\chi) \quad (5)$$

Eq. 5 takes into account that the photographic magnitudes relate to visual estimates according to $m_v = 0.71 \times m_{ph} + 1.30$ for the range of magnitudes (m_v = -0.5 to +2.5) over which the $sin(h_r)$-dependence was derived (Jacchia et al. 1967). The theoretical value from Eq. 4 and Eq. 5 is listed in Table 2. The results are in good agreement with the values derived from the observations.

I have adopted γ = 1.4 for all meteor streams, and a minimum radiant altitude of 10 degrees.

3.4. Observer perception

The observer dependent correction allows for systematic differences in rate counts among observers. These are mainly due to different detection limits and different observing techniques (concentrating on a small field of view in the center of vision or watching the entire sky).

I chose to normalise the counts assuming a similar probability function for stream and sporadic meteors, by comparing the observed sporadic rates to a canonical value of 10 meteors/hr at 0^h local time in early August (or early March in the southern hemisphere). The choice of date and local time is because of daily and annual variations of the sporadic flux. These variations are small in this part of the day and in this part of the year

(Srirama Rao et al. 1978; Hughes 1978) and observations are abundant.

c_p is defined as the ratio of true observed sporadic hourly rate (corrected for limiting magnitude, r = 3.4) and a standard value of HR = 10:

$$c_p = \frac{HR}{10} = \frac{n_s \times r^{6.5-Lm}}{10 \times T_{eff}} \quad (6)$$

The choice of 10 sporadic meteors per hour defines, in first order, a standard observer's probability of detecting meteors (see Appendix). c_p varies between 0.4 and 2.5 and has a median value close to 1.0 (= no correction). Values are listed in Table 1. I do not allow for a χ dependence in this correction factor and it is assumed that the observers do not change their observing techniques while at different locations. The relative sporadic rates indicate that this was - with a few exceptions - the case. This rather rough correction aligns the meteor counts to within some 20% typically (from a comparison of activity profiles of the Perseids: Jenniskens 1989a). The perception coefficients were found to vary little from year to year with a one sigma spread of about only 8% (Table 1).

Figure 3 shows the annual variation of sporadic activity after correction for observer perception. The sporadic meteors are all those meteors that are not from one of the radiants listed in Table 3. The southern hemisphere has almost constant rates, while the northern hemisphere has lowest rates in spring ($\lambda_\odot$ = 30) and highest rates in autumn ($\lambda_\odot$ = 230). This annual variation is mainly due to the position of the ecliptic, with sporadic activity being higher for a higher position of the ecliptic on the sky (dashed line in Fig. 3). The observed peak-to-peak variation is not large: only some 40% at +52N. (It is not excluded that the rates are affected by variations in observer perception, due to observers who try a bit harder in the quiet season.)

The sporadic rates are not much affected by the selection of minor streams from the sporadic background. The average HR is around 9-9.5, slightly less than 10, due to the use of a median c_p value and a skewness of the c_p distribution to high values.

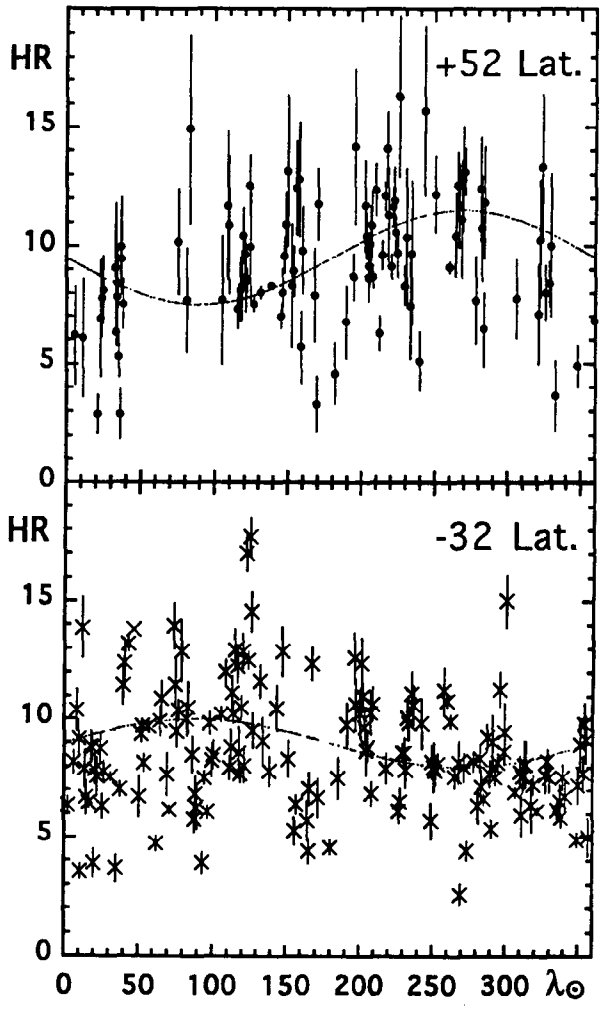

Fig. 3. Annual variation of sporadic activity $HR = n_s/(c_p T_{eff})$ on southern and northern hemisphere. The rates are averages of rates between local time 22:00 h and 04:00 h

3.5. Distance between center of vision and the radiant

The observed rates depend strongly on the angular distance between center of vision and the radiant (D). There is an optimum at about 35 degrees distance and rates drop quickly for distances beyond 90 degrees. Wood (1986) suggested the relation shown in Fig. 4. This is compared to the number of meteors photographed by a series of 21 small F2/50mm cameras that homogeneously covered the sky above 15 degrees altitude during the summer campaign in 1989 from Meterik in the Netherlands (ter Kuile 1989). The data are in good agreement. The first two points of photographic data are most severely affected by the difference between the integrating properties of photographic film and the human eye and can be neglected in the comparison with the proposed dependency for visual counts. Visual observers are alerted by movement and see less meteors when observing straight at the radiant than by observing D = 35 degrees away from it.

Because the center of vision is usually within 60 degrees from the radiant, no additional correction of the rates is needed. However, observers may occasionally have watched further away from an active radiant, for example, when observing several streams simultaneously. This can cause a systematic underestimation of rates up to a factor of two.

3.6. Year to year variations in meteor activity

Evidence has accumulated that the rates of the major stream vary from year to year. However, many reports of such variations are the result of instrumental effects and variable observing conditions. With the exception of meteor outbursts that are associated with recent cometary ejecta (Jenniskens 1994), large annual variations in meteoroid flux along the mean orbit of the stream are not likely, because the dispersion in meteoroid velocities is such that any density variation along the orbit of the comet is smoothed out in tens to hundreds of years (i.e. Murray et al. 1980).

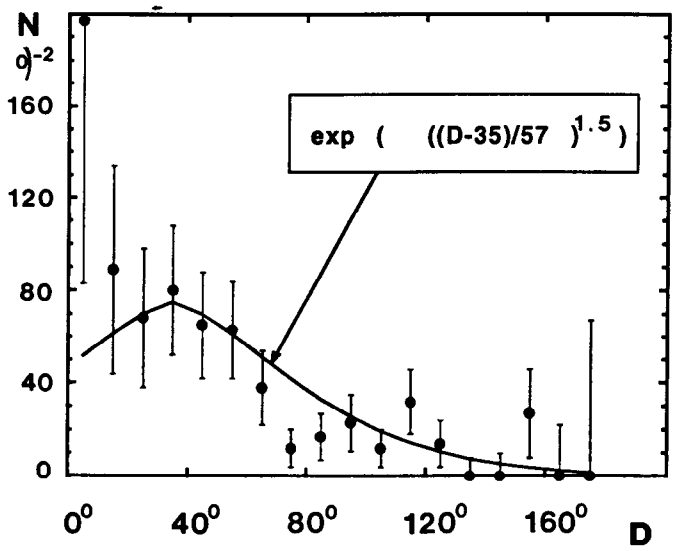

Fig. 4. Rates as a function of the angular distance (D) between the center of vision and the radiant. A functional dependence suggested by Wood (1986) is compared to the number of photographed meteors by a system of 21 small cameras that covered the sky homogeneously above 15° altitude during a Perseid campaign (ter Kuile 1989)

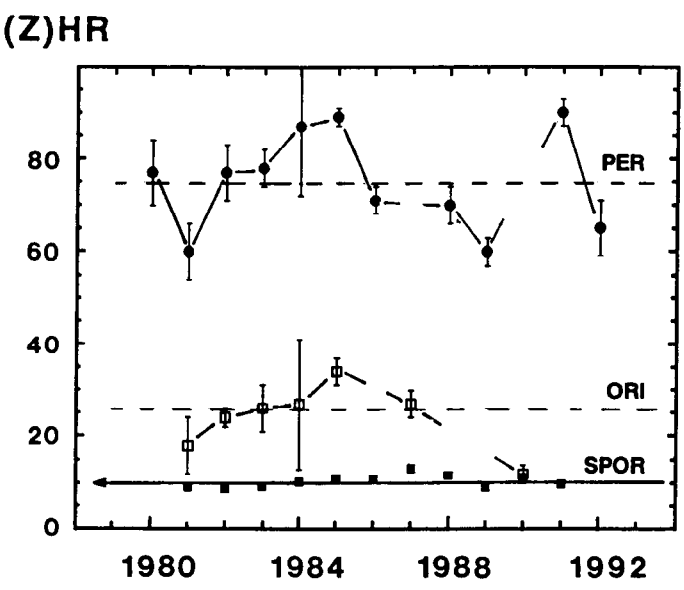

Fig. 5. The year to year variation of peak activity of the Perseids, Orionids, and sporadics. Data for the Perseids of 1980 are discussed in Jenniskens (1992b)

Annual variations of the peak activity of some major streams have been reported at the level of 20-50%, and have been linked to conditions in the upper atmosphere, notably to variations in the density gradient at altitudes near 100 km (Lindblad 1968; Hughes 1974; Ellyett 1977). The density at a given altitude in the upper atmosphere is found to decrease up to 35% during a geomagnetic storm and by 10-15% following a geomagnetic disturbance. Lindblad (1978) found this to directly affect meteor radar rates by 20-25%. A decrease in density gradient will result in a lower peak brightness (Δm) for a meteoroid of given mass and entry conditions, which again may result in lower detection rates by about a factor $\chi^{\Delta m}$. Alternatively, planetary perturbations by Jupiter have been proposed as the cause of the small periodic variations in meteoroid flux density (i.e. Hajduk 1986). The 12 yr period of Jupiter comes close to the 11 yr periodicity in solar activity, which affects the upper atmosphere conditions. However, currently there is no evidence that Jupiter is the cause of the variations. Finally, detectable variations in stream activity are expected when the geometry of Earth orbit and meteoroid orbits changes quickly. For example, the Bootids and Geminids are swept by the Earth's path over a timescale of 100 yr (Murray et al. 1980; Fox et al. 1982). But this process is so slow as not to affect the relative rates over the 11 year period considered here.

Figure 5 shows the Perseids and Orionids for individual years between 1981-1991 (which covers one solar cycle from max. to max.). The rates of these streams are, again, found to vary by typically 20% from year to year. Peak rates occurred in 1985 during solar minimum. Previously, peak acitivty was noticed in 1963 and possibly in 1953 (Lindblad 1968, 1980; Hughes 1976; Zvolankova 1984) from which a period of 11 yr follows and a period of 12 yr is excluded.

For the other major streams, for which fewer returns have been observed, I find no significant variation from year to year, that is, over a factor of two or more, with the exception of occasional meteor outbursts, like those of the Lyrids in 1982 and the Ursids in 1986. Meteor outbursts are rare and stand out clearly from the annual activity. From this result I make the assumption that the rates of the minor streams, similarly, do not vary significantly from year to year. This justifies the combination of data from several returns in order to gain in statistical weight.

3.7. Discussion of uncertainties

Adding data of several returns decreases the statistical error in the counts, but at some point other random errors, or worse, systematic errors become the dominant limiting factor.

The statistical error in the meteor counts, which have a Poisson distribution, is given by:

$$\sigma ZHR = ZHR/\sqrt{(N)} \qquad (7)$$

where N is the total number of observed stream meteors. For N = 1 the best estimate of the ZHR is at 2/3 times the calculated value.

For large enough N systematic errors become dominant. After correction for limiting magnitude, observer perception, and radiant altitude dilution, which all carry a limited accuracy, there remain uncertainties due to possible changes of observing technique, lack of concentration, a viewing direction far away from the radiant, etc. For a large enough dataset these may act as random errors, but that is not at all certain. For example, minor streams are often observed during the activity of a major stream. In that case, there may be a systematic constraint on the viewing direction with respect to the radiant.

The activity curves are sensitive to meteor classification errors. The contamination by sporadic meteors in the counts due to chance alignment has been estimated by Koschack (1991),

who found that 3-5 % of sporadic meteors are classified as a stream member for a chosen radiant position at altitudes 30-60 degrees, and V_∞ = 30 – 60 km/s, and a radiant diameter of 10 degrees. This limits the minimum detectable Zenith Hourly Rate to about 1 and overestimates the rates at a low level of activity. On the other hand, due to plotting errors a percentage of stream meteors are not counted as such, depending on the location of the center of vision relative to the radiant. For a distance of 30 degrees from the radiant, about 7% of meteors may be wrongly classified; for a distance of 60 degrees this may be as much as 25% (Koschack 1991).

The detection limit of a meteor stream is a complex function of, for example, the position of the radiant on the sky, the difference between entry velocity of meteor stream and sporadic background, and the presence of nearby meteor streams with similar entry velocity. The minor streams listed in Table 3 are the ones that stand out most clearly.

4. The shape of the activity curves

Zenith Hourly Rates are calculated for each observation, which then are averaged over an interval in solar longitude ($\lambda_\odot$) in order to arrive at rate estimates of about equal statistical weight. The ZHR data are plotted on a single-log scale against $\lambda_\odot$ (equinox 1950.0). Several of the major streams are shown in Figs. 6-9, all other streams in Fig. 11. Southern hemisphere data, from NAPO-MS members, are given by crosses, while the northern hemisphere data, from DMS members, are given by dark points. The individual points are not smoothed by a sliding mean, because that may affect the slopes of the ZHR curves, but instead are averaged over an interval in solar longitude not exceeding 1 degree. This retains full time resolution (1 hour intervals) if indicated by the density of points. Error bars are according to Eq. 7, where N is the total number of observed meteors in an interval of solar longitude.

4.1. The Perseids

The *Perseids* is the best studied stream, because meteors appear during summer holiday in the northern hemisphere. In total, 14,635 meteors are selected for the construction of the activity profile in Fig. 6.

The data can be compared to the fairly completely sampled Perseid results of Denning (1898), Zvolankova (1984), Lindblad (1986), Veltman (1983b, 1984, 1986b), and Mason & Sharp (1981), which is done in (Jenniskens 1986). There is good agreement between these visual results and the radar data by Simek & McIntosh (1986) and Lindblad & Simek (1986). The activity profile is well represented by four straight lines in a log–normal plot:

1 Between 120 and 137° there is a nearly exponential increase of activity (a linear increase in Fig. 6) with a slope (B) of B = 0.050±0.005 in log(ZHR) per degree of solar longitude up to a level of activity of ZHR = 18 at $\lambda_\odot$ = 137.0. There is some evidence that the slope may be somewhat steeper below $\lambda_\odot$ = 130 (B ~ 0.057) and shallow between $\lambda_\odot$ = 130 and 137 (B ~ 0.017).
2 The main peak is essentially symmetric with, again, exponentially increasing and decreasing branches (B = 0.20±0.01 °)$^{-1}$). There is no evidence of stable submaxima in the peak profile as suggested by Roggemans (1989). The centeroid is at $\lambda_\odot^{max}$ = 139.44±0.03 (weighted mean between $\lambda_\odot$ = 137.1 and 141.7). The mid-point between levels of half the peak value is at $\lambda_\odot$ = 139.43.
3 Between 142 and 152 degrees is a fast exponential decrease in activity starting from ZHR = 17 at $\lambda_\odot$ = 141.8 with a slope of 0.083±0.017 °)$^{-1}$, but this value depends heavily on some low rates observed near $\lambda_\odot$ = 152.

These values for slope and peak activity are listed in Table 3b. A good fit to the curve can be obtained by a sum of two sets of exponential curves (as shown in Fig. 6). In that case the slopes of the main peak come out a bit steeper: B = 0.35 and (ZHR_{max} = 70) and the background component has B^+ = 0.050, B^- = 0.092 (ZHR_{max} = 23). Note that this fit does not account for a possible shoulder near $\lambda_\odot$ = 130 (Fig. 6).

The nodal regression of the orbit can be derived by comparing the centeroid of this profile with that of Denning (data from 1868-1896; mean 1885) and the weighted mean time of maximum given by Zvolankova (1946-1953), Lindblad (1953-1981), and Mason & Sharp (1980). These values are respectively $\lambda_\odot$ = 139.31±0.08, 139.22±0.08, 139.28±0.03, and 139.33±0.05. This suggests that there are significant variations of the node of the Perseids on a timescale of 100 yrs, with a positive shift of some 0.0047±0.0005 °/yr in recent years. However, historic records of Perseid returns indicate that over long periods of time (t) the node remains fairly constant. Over the past two millenia Hughes (1982a) has: $\lambda_\odot^{max}(1950.0)$ = 138.48 + 0.00038 ± 0.00027(1950.0 – t(yr)).

4.2. The Geminids

Another example of a stream with a definite background tail in activity is the *Geminids*. The Geminids are as active as the Perseids, but observations are hampered by bad weather conditions during the winter. The northern hemisphere data are mainly from 1990 and 1991. The stream is observable from the southern hemisphere, although under less favorable conditions. The calculated ZHR values from northern and southern hemisphere data are found to deviate by 35%.

Again, the profile is well represented by exponential slopes. However, contrary to the Perseids, and most other streams, there is clear evidence for asymmetry in the main peak, with a shallower ascending branch. A fit to the main peak gives: B^+ = 0.39±0.04 and B^- = 0.72±0.10. A decomposition in two components with exponential slopes centered at the peak position gives B^+ = 0.59±0.07 and B^- = 0.81±0.10 (ZHR_{max} = 74) for the main peak. The asymmetry in the peak may reflect the way particles are lost from the parent body. Fox et al. (1982) showed that the pre-peak material is probably ejected at anomalies between 0-135 and post-peak material contains somewhat

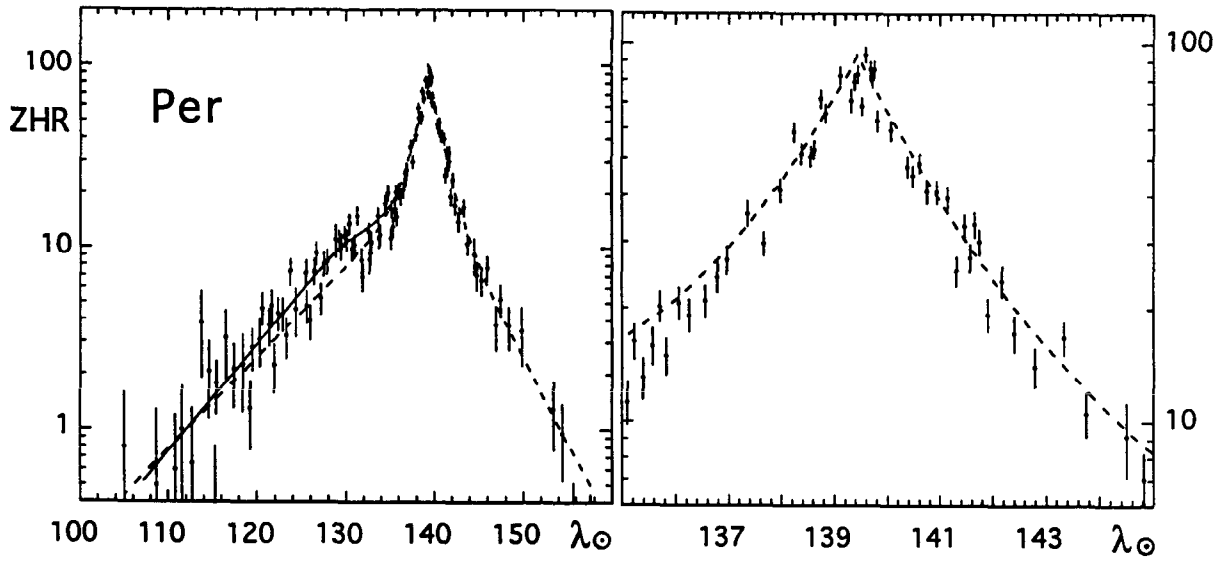

Fig. 6. The Perseids

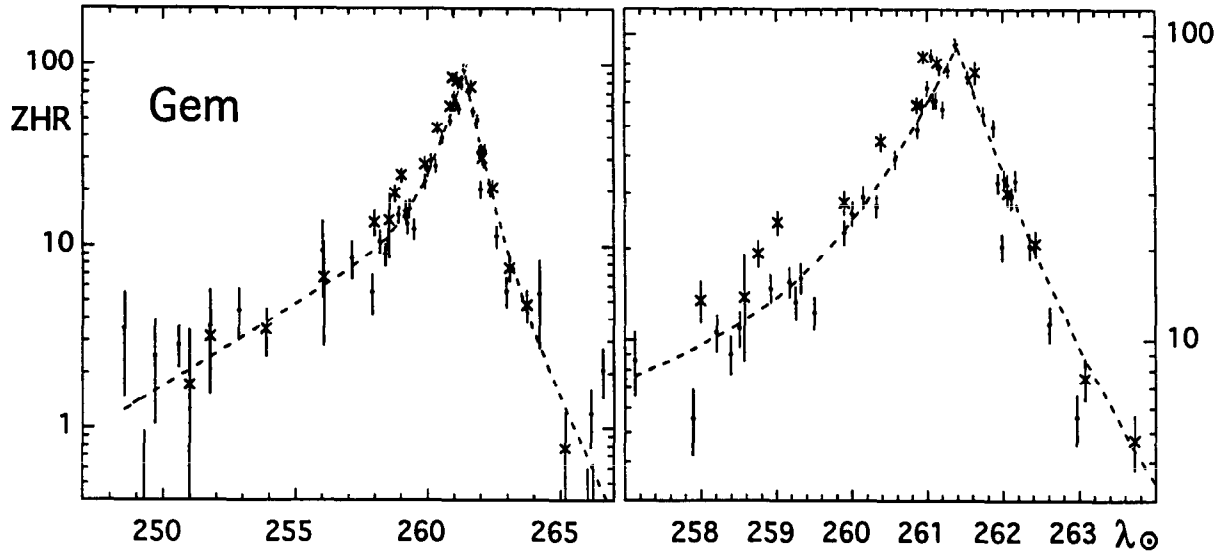

Fig. 7. The Geminids

more material ejected between anomalies 180 and 225. Alternatively, planetary perturbations can account for an asymmetry, although there is no sign of the hollow structure that was found in the modelling (Jones 1985). The effect of radiation forces is discussed in Olsson-Steel (1987).

McIntosh & Simek (1980) found a relationship between the time of maximum and meteor magnitude: $\lambda_{\odot}^{max} = 261.3 - 0.135m$. This result is confirmed from visual observations by Spalding (1984), who considered meteor rates averaged over time intervals of 0.25 days and found: $\lambda_{\odot}^{max} = 261.55 \pm 0.05 - 0.078 \pm 0.025m_v$. Simek (1978) found from radar data that the maximum for given meteor magnitude is at: 260.54±0.11 (+6), 261.17±0.07 (+1.8) and 261.39±0.09(-1.3), which results in $\lambda_{\odot}^{max} = 261.29 - 0.118m_v$. A combination of the activity curve and the change of χ over time suggests that the true maximum doesn't change very much, but the skewness of the profile is magnitude dependent. The time of maximum derived from fitting exponential slopes to the data hasn't shifted significantly in 15 yrs: $\lambda_{\odot}$ = 261.4±0.2 (1969-1980, Spalding 1982), $\lambda_{\odot}$ = 261.4±0.1 (1990-1991, our data). There is no evidence of a significant shift of the node since the discovery of the stream in the beginning of the 19th century. The peak in activity remained within error at 261.3±0.2 (Spalding 1982), i.e. $d\lambda_{\odot}/dt < 0.002\ ^{\circ}$/yr.

4.3. The Orionids

Most streams satisfy a single set of exponential slopes. One example is the *Orionids*, which has a symmetrical profile: rising and falling ZHRs have a slope of $B^+ = 0.122$, $B^- = 0.098$ in the northern hemisphere data, and $B^+ = 0.140$, $B^- = 0.140$ in the southern hemisphere data. By folding the data around the time of

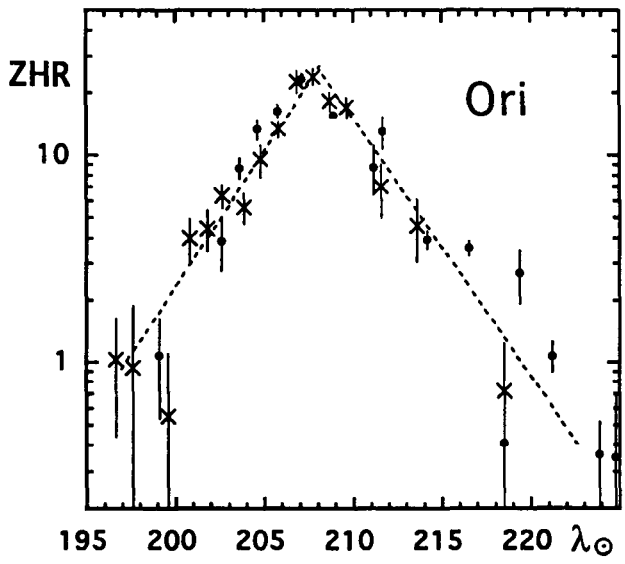

Fig. 8. The Orionids

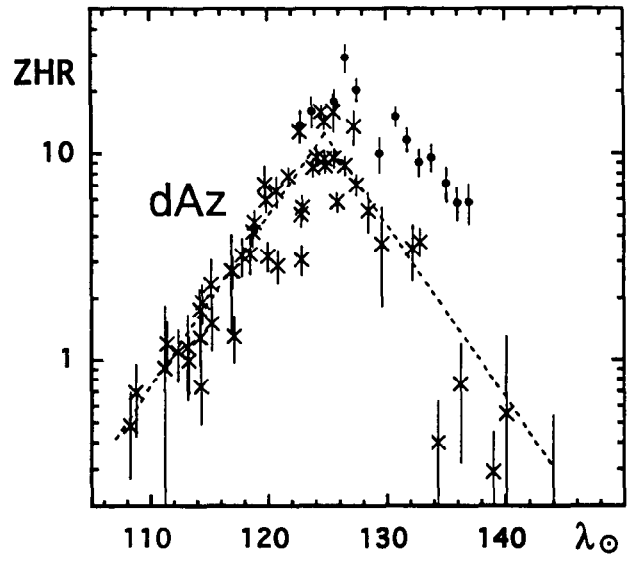

Fig. 9. The Delta Aquarids

maximum, and averaging, a mean value of B = 0.105±0.012 is obtained because the northern hemisphere data after maximum are abundant and put large weight in the result. The southern hemisphere data suggest that this value of B may be slightly underestimated. I adopt B = 0.12. The absolute zenith hourly rates from northern and southern hemisphere observers agree well.

The profile is in good agreement with Spalding (1987). Again, I find no support for stable maxima in the profile as reported by Stohl & Porubcan (1978), Hajduk (1980), Cevolani & Hajduk (1987), Hajduk (1986), and Porubcan et al. (1991). A stable maximum meaning that subpeaks are present in the profiles of several subsequent returns at a stable position in solar longitude. Note that error bars are not normally shown in the published data. Most of the reported peaks may be due to instrumental variations and small number statistics. Although the existence of filamentary structure was one of the arguments used in favour of the Ribbon Model by McIntosh & Hajduk (1983) and McIntosh & Jones (1988), the model does not necessary imply such filamentary structure. An important result in favour of a Ribbon Model for the Halley streams is the similar width (B = 0.080±0.014 and 0.12±0.02 respectively) and the relative level of activity for η Aquarids and Orionids. Notably, the η Aquarids are only slightly stronger than the Orionids (ZHR_{max} = 37 and 25 respectively).

4.4. The Delta Aquarids

The worst cases with respect to an agreement between southern and northern hemisphere observers, are the streams of *Capricornids* and *Delta Aquarids*. Figure 9 shows the δ Aquarids. The profile is well represented by a single set of exponential slopes and the profile is symmetric, but the northern latitude observers (descending branch only) find systematically a factor of 3 higher rates. This is the most deviant case in terms of agreement in absolute values between southern and northern hemisphere data. The same deviation is found for the Capricornids, for which relative conditions are comparable (Cap, Fig. 11).

The δ Aquarids are observed under very different conditions from northern and southern latitudes. While the radiant is almost in the zenith from southern latitude -32, the radiant stays below 26 degrees altitude at latitude +44 (South of France), where most of the northern hemisphere data for this stream are gathered. γ = 0.6, instead of γ = 1.1, would explain the large difference from an effect due to the radiant altitude correction, but this value seems unreasonably low. I suspect that the difference is due to classification errors, where more sporadic meteors are classified as Aquarids or Capricornids at northern latitudes. It is surprising, though, that the slopes of the resulting profiles are so similar for both groups of observers.

4.5. The Bootids

Few data are available for the *Bootids*, or *Quadrantids*, a major stream that occurs in early January, often in bad weather conditions. The stream is exceptionally narrow (e.g. Hughes et al. 1979). Most of the stream's activity variation occurs in a single night, during which the radiant has a lower culmination at low altitude in the late evening and rises high up in the sky in the early morning. As a result, there are quick variations of the various correction factors and, consequently, many observational data reported in the literature are seriously in error.

The stream has been studied extensively by radar. The most thorough study is that by McIntosh & Simek (1984). These data do not show a profile that is well represented by two exponential slopes (Fig. 10). The data in all three groups of echo durations seem to be saturated in the peak of the profile between $\lambda_\odot$ = 282.40 and 282.75. Surely, this is a perfect example of data not agreeing with the assumption that emerges from the analysis of previous ZHR curves: that all streams obey linear slopes in log–normal curves. However, data of Bel'kovich et al. (1984) do not show this "saturation", while ascending and descending

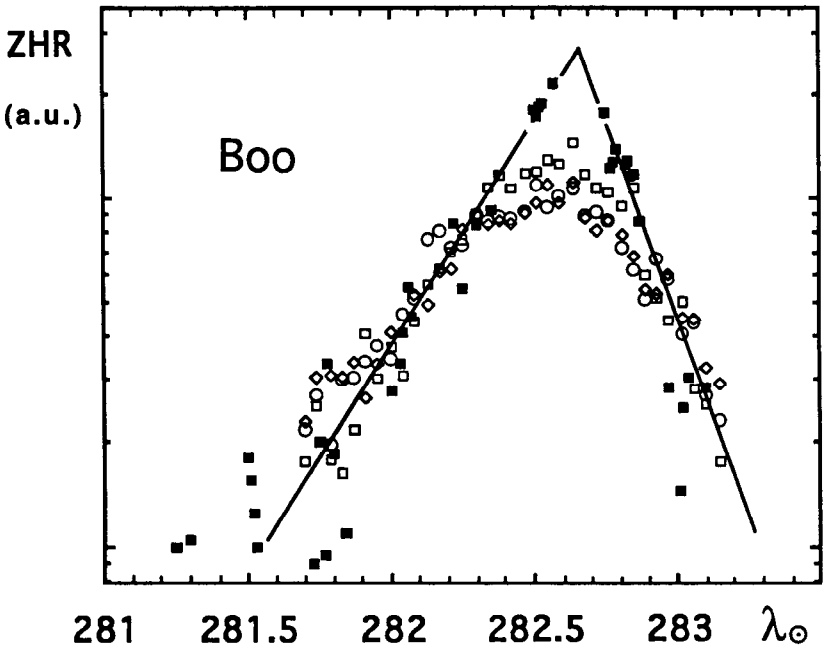

Fig. 10. Radar data for the Bootids. Open symbols: McIntosh & Simek (1984), closed squares: Bel'kovich et al. (1984). The former data show saturation between solar longitudes 282.40 and 282.75

branches agree well with McIntosh & Simek in the "unsaturated" part of their data, where $B^+ = 1.29$ and $B^- = 2.28$ (Fig. 10). Also data of Poole et al. (1972) do not show signs of saturation ($B^+ (= B^-) = 1.5$, $\lambda_\odot^{max} = 282.60 \pm 0.08$). I conclude that the Bootids, too, are well represented by a set of exponential slopes and that, indeed, the detection of Bootids by McIntosh & Simek is saturated in the peak of the profile. Note from their figures that the real peak is reduced to a minor increase. The time of maximum is at 282.64±0.02 (data obtained between 1958 and 1981).

The visual data, shown in Fig. 11, agree well with the radar data concerning the width of the stream. The data have been complemented with results by Nolle & Koch (1988), shown by open symbols in Fig. 11. I find a fairly symmetric profile with B = 1.8±0.4 and a peak at $\lambda_\odot$ = 282.62±0.03 (for data centered on 1987). Recent results from the return of 1992 by Rendtel (1993b) have a peak at $\lambda_\odot$ = 282.51±0.04 and slopes B^+ = 1.4±0.2 and B^- = 2.2±0.7, while similar data from 1989 give: $\lambda_\odot$ = 282.67±0.06, B^+ = 1.1±0.2, B^- = 1.6±0.2. These data suggest a similar skewness in the profile than found for radar data and a difference in time of maximum with respect to the radar data of less than $\Delta\lambda_\odot = 0.15^o$. These results are at odds with data by Hindley (1971), who has typically a steeper decending branch and a peak position shifted to higher solar longitude: $\lambda_\odot$ = 282.82±0.04 (1970 and 1971) and slopes B+ = 1.66, B^- = 2.56 (1970) respectively B^+ = 1.19, $B^- \sim 5$ (1971), suggesting that $\Delta\lambda_\odot \sim 0.26^o$ (e.g. Hughes et al. 1979). It is possible that there are significant variations from year to year around the mean position, but the results are very sensitive to the reduction procedure and should be interpreted with care.

By combining the times of maximum activity derived from visual data listed in Prentice (1953) and Hughes et al. (1979), I find a nodal regression of: $\lambda_\odot^{max} = 282.81 \pm 0.03 - 0.0048 \pm 0.0007(1950.0 - t(\mathrm{yr}))$, which gives a good fit to the data of the Bootids since their discovery in January 1835. This value is close to the maximum value calculated from theory by Hughes et al. (1981). Evidence that the nodal regression for visual meteors is different from that of radio meteors (i.e. Hughes et al. 1981) is weak.

The Bootids do show a background activity similar to the Geminids, but the slopes before and after maximum are ill defined in our data. The adopted values in Table 3c agree with more extensive data by Nolle & Koch (1988) and Rendtel et al. (1993b).

4.6. Conclusions

In conclusion, all meteor streams discussed in this section are in first order well respresented by linearly ascending and descending branches if plotted on a logarithmic scale, i.e.:

$$ZHR = ZHR_{max}\ 10^{-B|\lambda_\odot - \lambda_\odot^{max}|} \quad (8)$$

Some streams need a combination of at least two of such curves. The main peak of most major streams is symmetric, that is, $B^+ = B^-$ (exceptions: Gem and Boo).

I checked whether a power law, like an r^{-2} dependence, could fit the data. Only the outer parts of, for example, Perseids and Orionids are represented equally well by an r^{-2} dependence. The inner part shows a much less steep decrease in activity, where the inner part for the Perseids is between 10 days before maximum and 3 days after, and for the Orionids between 3 days before and 4 days after peak activity.

5. Results for other streams

Figure 11 shows the ZHR data of the other 45 streams, in a similar format as before. I assume that most other streams are also well represented by a (single) set of exponential curves.

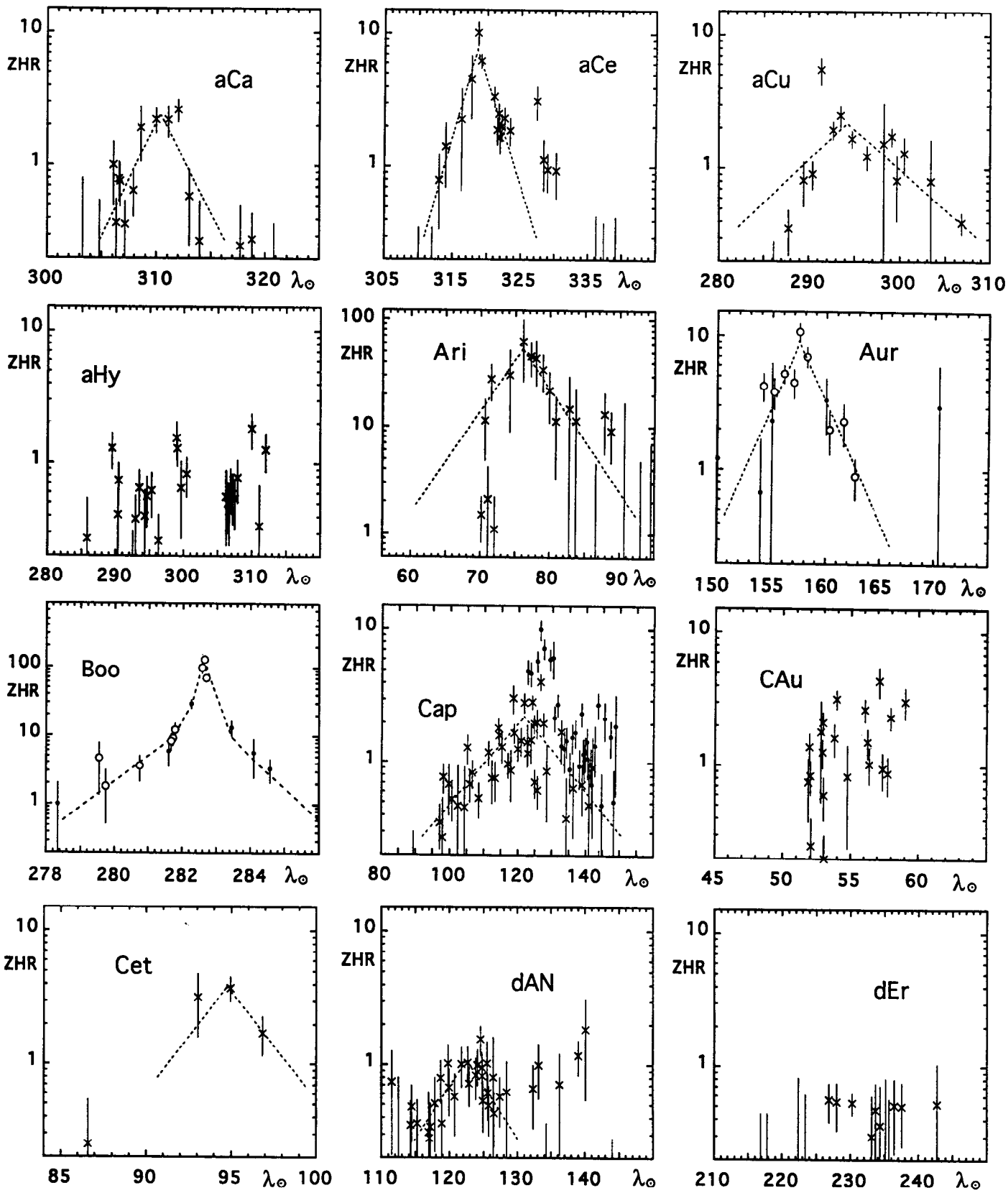

Fig. 11. Meteor stream activity curves of all other streams not shown in Figs. 6-9. Crosses refer to data by NAPO-MS members (southern hemisphere) and dark points are data by DMS members (northern hemisphere). The results for Bootids (Boo), Aurigids (Aur), and Ursids (Urs) are complemented with results of Nolle & Koch (1988), Rendtel (1990b), and results from other DMS observers respectively. These data are shown by open circles

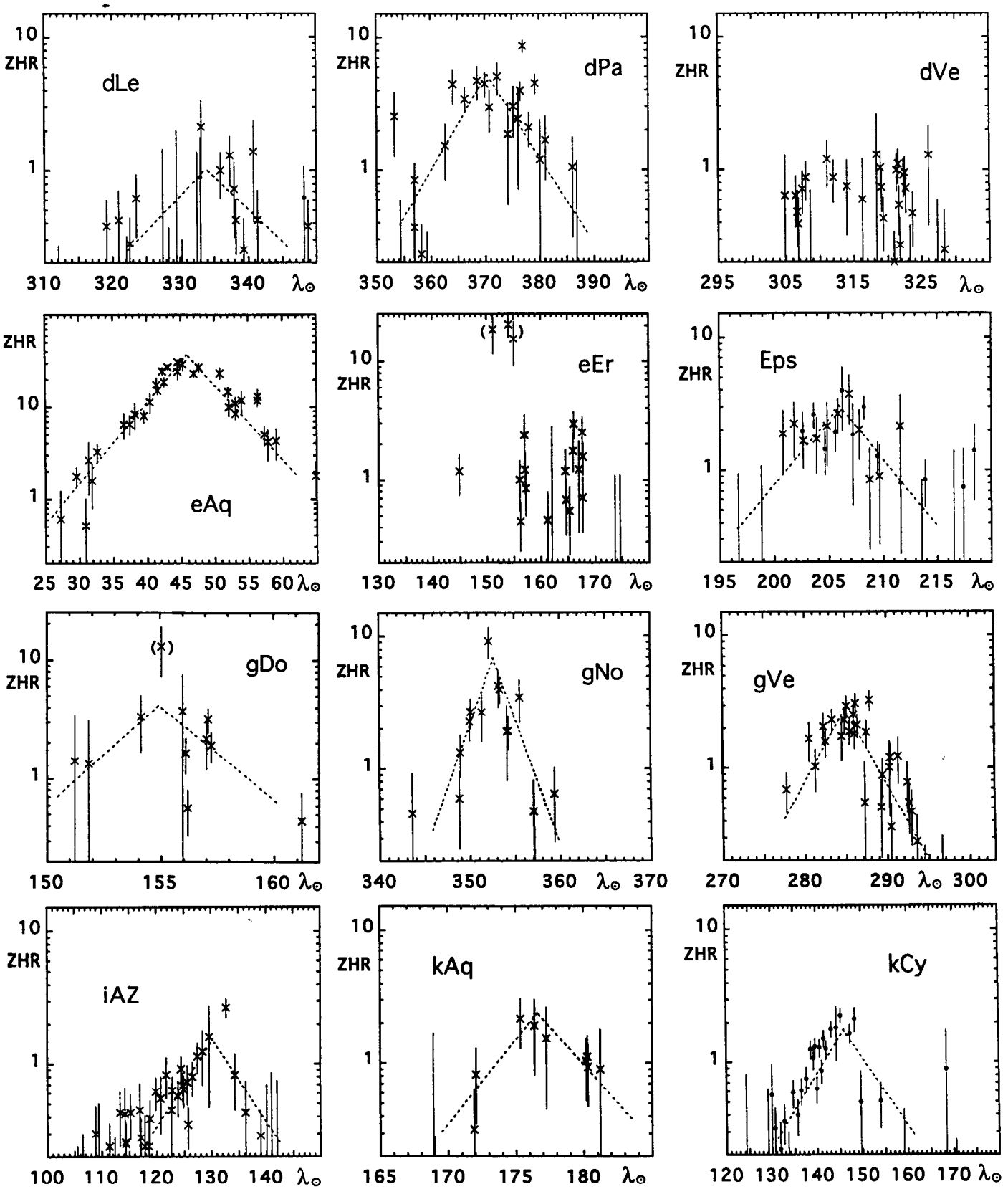

Fig. 11. (continued)

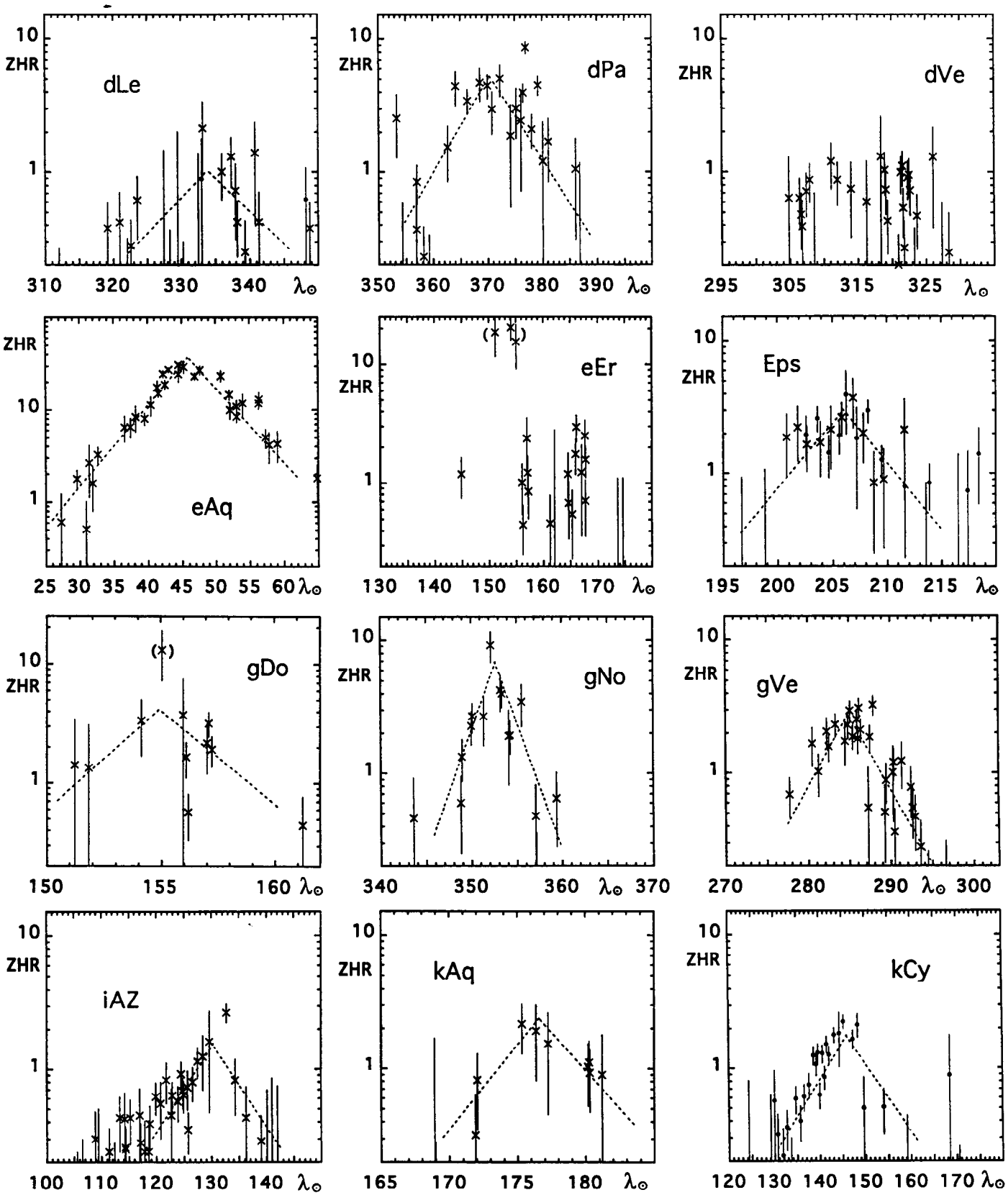

Fig. 11. (continued)

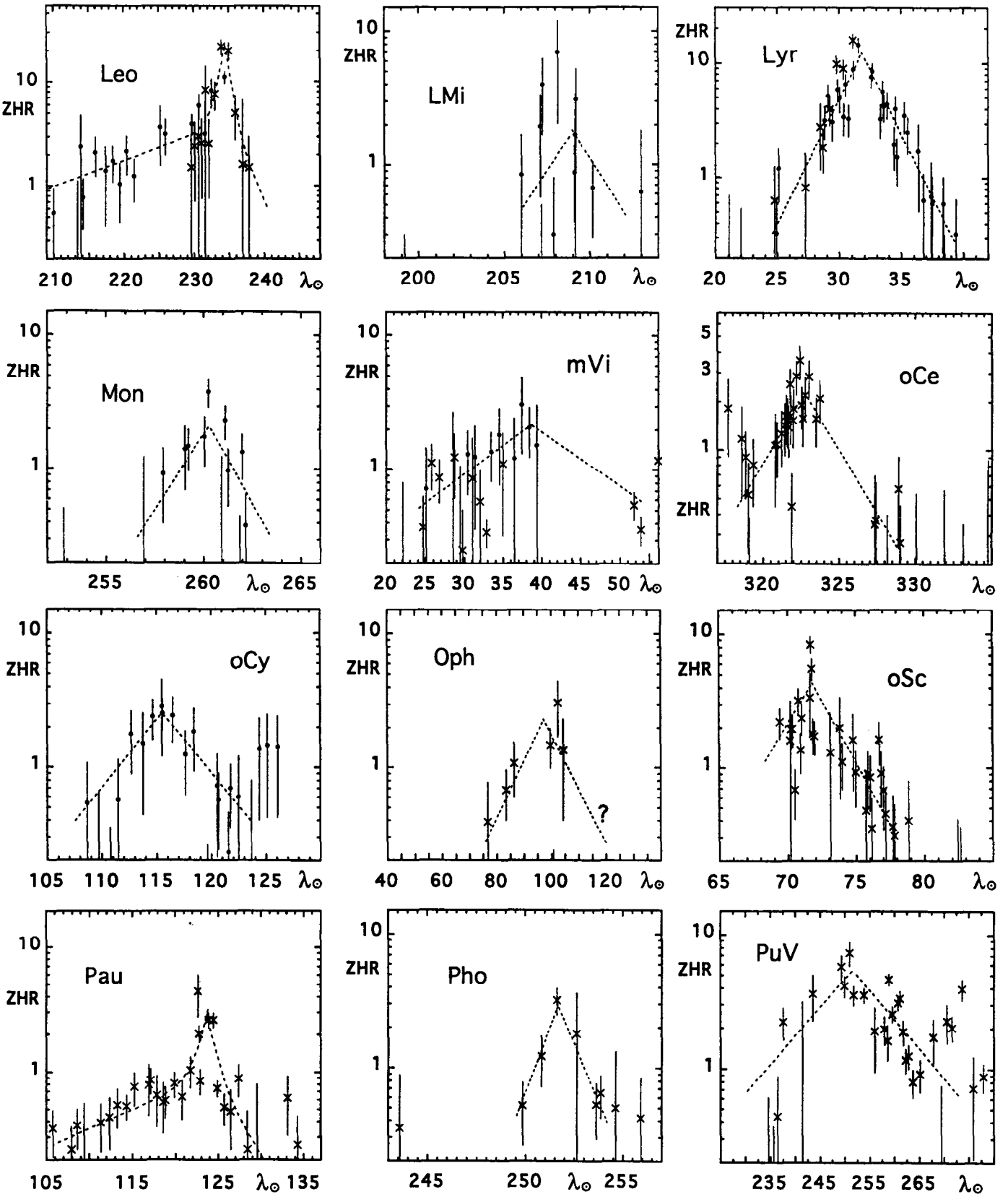

Fig. 11. (continued)

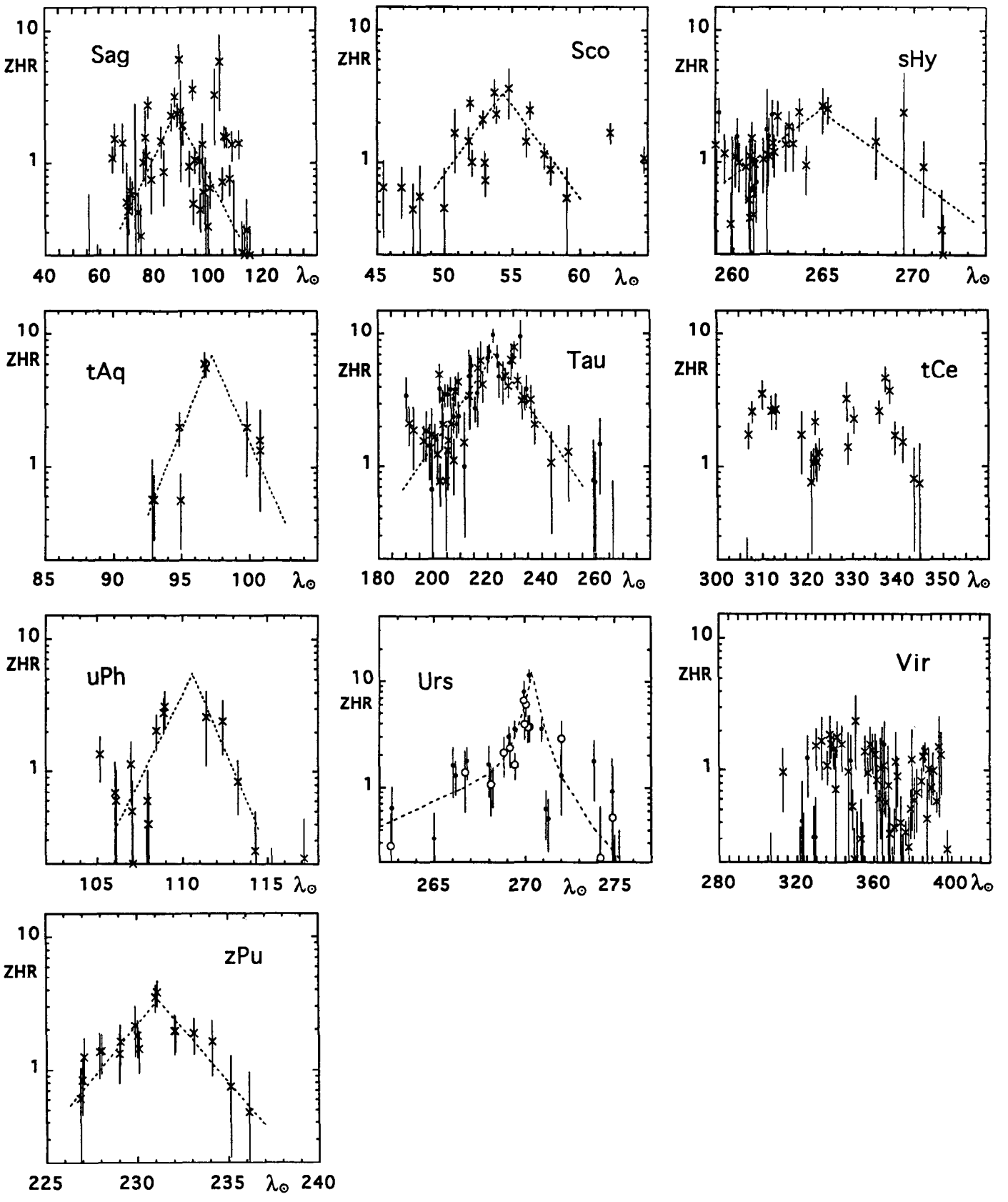

Fig. 11. (continued)

Statistical weight is gained by folding the data around time of maximum activity $\lambda_{\odot}^{max}$. Thus, an average value of B is obtained from a least-squares fit to the data in a log–normal plot. Values for $\lambda_{\odot}$(max), ZHR_{max}, and B of all streams are tabulated in Table 3b. These values refer to a fit to the data of the main peak. For those streams where a background component is detected, a decomposition is made (Table 3c).

5.1. Discussion of individual streams

Seven streams out of 50 do not allow an acceptable fit, in all cases because the rates do not rise much above the detection limit set by classification errors (aHy, dVe, tCe, Vir, Oph, eEr, and dEr).

In two cases I was in doubt whether to choose one or two components. Evidence for a tail in the *Ursid* stream is weak, because of a lack of observations. The slope of the main peak (B = 0.61) is unusually high. A single set of exponential curves would have $B^{+} = 0.20$, $B^{-} \sim 0.62$, and $ZHR_{max} = 6.2$ at $\lambda_{\odot}^{max} = 270.35$. The *Pisces Australids* are a minor stream of long duration. Some observations around July 27th suggest that superposed on a wide background of activity there is a prominent peak of B~0.26, but the peak is not well observed.

Some other cases suggest a complex of streams, with several maxima from different radiants during an extended period of time. The *Virginids* do not show a well defined activity profile. ZHRs remain low. The *μVirginids* stand out from the αVirginids and other branches in late April and early May in that the meteors are somewhat faster in angular velocity and radiate from a point more in the direction of Libra instead of Virgo. Rates are too low to have a meaningful discrimination of even more radiants. Another example is the *Puppids/Velids* complex, with several radiants in Puppis and Vela. Photographic data show the presence of a stream of μVelids at solar longitude $\lambda_{\odot}$ = 262; RA,DEC = 155,-41; and V_{∞} = 55 km/s (Jacchia & Whipple 1961; McCrosky & Posen 1961). Nilson (1964) and Gatrell & Elford (1975) observed several meteors from this region of the sky by radar, notably from (262; 143,-44; 38 km/s - the γVelids II), (257; 140, -50; 41 km/s), and (262; 135, -63; 35 km/s). It is not clear if these radiants produce significant activity in the visual range. In addition, Jeff Wood discriminates from visual observations the σPuppids (225; 102,-45; 38 km/s), the τPuppids (272; 104,-50; 33 km/s), the ζPuppids II (251; 123,-43; 41 km/s), the c-Velids (273; 135,-46; 38 km/s), and the πPuppids (290; 113,-43; 35 km/s) (Rendtel 1990a). Obviously, care should be taken when interpreting the PuV activity curve.

The data of some other streams do show a well defined profile, but are less reliable than the activity trends suggest. The ZHR of the *ωScorpiids* near maximum may be affected by some systematic error as they are based on one observer and one night only. The same is true for the *γ Dorids* (gDo) and the *ϵ Eridanids* (eEr). If the latter stream is associated with the new (e = 1.00025, Marsden 1983) comet Kinkerfues 1853 III, then a maximum is expected at $\lambda_{\odot}$ = 169 instead of 152 (Drummond 1981).

Also, care should be taken with the solutions for the ϵ Geminids and Monocerotids. The *Monocerotids* have a radiant close to that of the Geminids, but are well observable in a butterfly shaped part of the sky north and south of the line that crosses the radiants (Jenniskens 1991). It is not clear if all observers did restrict themselves to this part of the sky. Activity peaks in the night before maximum activity of the Geminids. The maximum of the *Epsilon Geminids* is found on Oct. 20, which is two days before the peak of the Orionids. The activity period coincides with the period over which meteors have been photographed: Oct 14-27, which gives some confidence in the final result.

The *Taurids* have a clearly defined northern and southern branch, with radiants some 7 degrees apart and significantly elongated along the ecliptic. From visual observations it is difficult to separate both branches. The available data of observers that make this discrimination show a similar curve for both streams, while the northern branch is slightly favoured over the southern branch (5:4). This is opposite to photographic evidence, where the southern branch is the more active one (about 2:1). Although both branches may have a different χ, it is more likely that the difference is due to classification errors, unless proven otherwise. Only combined data are shown here.

The *Arietids* are a daylight stream, but give some visible meteors in the hour after both evening twilight and before morning dawn. The radiant altitude is typically below 10 degrees. The ZHR calculation leads to a reasonable result only after correction for zenith attraction (Eq. 4). This may affect the scale of absolute values. The resulting profile has a peak position close to that of the radar data by Lovell (1954). The δ Aquarids have similar orbital elements and may be related. The stream has a width very similar to that of the δ Aquarids. Judging from the relative level of activity, the Earth passes closer to the center of the stream during the Arietids ($ZHR_{max} \sim 54$) than during the δ Aquarids ($ZHR_{max} = 11.4 \pm 1.2$).

5.2. The stream cross section

Figure 12 shows the equivalent cross section of all streams as a function of inclination (i). Only those streams are included that resulted in a confident estimate of B (39 streams). The equivalent cross section is defined in Eq. 25 (Appendix) and in appropriate units is given by:

$$\begin{aligned} \Delta t(^{\circ}) &= 0.869/B \\ \Delta t(\text{days}) &= 0.881/B \\ \Delta t(AU) &= 0.0152/B \end{aligned} \qquad (9)$$

The distribution of effective cross sections peaks at Δt = 0.08 AU, which corresponds to Δt = 4.6 days and B = 0.19. At a distance of 0.08 AU from the center of the stream the activity is a factor of $e^{-2} = 0.14$ less. It may be no coincidence that as a "rule of thumb" (McIntosh 1991) comet orbits have to approach the Earth's orbit to within about 0.08 AU in order to give a detectable meteor stream (Drummond 1981). I conclude that the stream cross section is fairly 'circular' for most meteor streams, with elliptical main and minor axis ratio's much less

Table 3a. The meteor streams that are discriminated in this study. The columns list, respectively, the common name of the stream, the radiant position (RA,DEC) at solar longitude ($\lambda_\odot$), the radiant drift ($\Delta RA, \Delta DEC$; in units of degree of arc per degree of solar longitude), the geocentric entry velocity of the meteoroids in the atmosphere which includes the Earth's gravitational acceleration (V_∞; in km/s), and the magnitude distribution index (χ). The final three columns list the number of stream meteors selected from the database, the total effective observing time involved (neglecting overlap of streams) and the number of observers who contributed to the data. *) χ varies with $\lambda_\odot$. The daily motion of the radiant is derived from photographic radiant positions (i.e. Krésak & Porubcan 1970, Cook 1973) or is calculated from the (parabolic) orbital elements by assuming a shift in the node only

Code	Name	$\lambda_\odot$	RA	DEC	ΔRA	ΔDEC	V_∞	χ	N	ΣT_{eff}	N_{obs}
Boo	Bootids	282	232	+45	+0.6	-0.3	43	*2.5	290	33	8
gVe	γ Velids	287	125	-47	+0.5	-0.2	35	3.0	386	208	6
aCu	α Crucids	295	192	-63	+1.1	-0.4	50	2.9	301	174	5
aHy	α Hydrusids	294	133	-11	+0.7	-0.3	44	2.8	164	197	5
aCa	α Carinids	301	95	-54	+0.4	+0.0	25	2.5	114	97	5
dVe	δ Velids	325	131	-52	+0.5	-0.3	35	3.0	147	186	5
aCe	α Centaurids	319	209	-58	+1.3	-0.3	57	2.3	297	199	6
oCe	o Centaurids	325	177	-56	+0.9	-0.4	51	2.8	247	215	6
tCe	θ Centaurids	325	210	-41	+1.1	-0.4	60	2.6	176	121	5
dLe	δ Leonids	326	160	+19	+1.0	-0.3	23	3.0	57	186	9
Vir	Virginids	354	177	+6	+0.9	-0.2	26	3.0	203	196	10
gNo	γ Normids	325	249	-51	+1.3	-0.2	56	2.4	138	97	6
dPa	δ Pavonids	9	308	-63	+1.6	-0.2	60	2.6	323	162	6
Lyr	Lyrids	31	272	+33	+1.2	+0.2	49	2.7	592	388	15
mVi	μ Virginids	35	227	-7	+0.5	-0.3	30	3.0	54	130	7
eAq	η Aquarids	45	338	-1	+0.9	+0.3	66	2.7	2925	191	6
CAu	β Corona Australids	56	284	-40	+1.3	+0.1	45	3.1	278	109	6
Sco	α Scorpiids	45	240	-25	+1.1	-0.2	35	2.5	902	482	6
oSc	ω Scorpiids	71	239	-20	+1.0	-0.1	21	3.0	261	109	6
Ari	daytime Arietids	75	45	+23	+0.7	+0.6	38	2.7	39	21	3
Sag	γ Sagitarids	76	271	-26	+1.1	+0.1	29	2.9	555	387	6
Cet	τ Cetids	96	24	-12	+0.9	+0.4	66	2.5	38	15	2
Oph	θ Ophiuchids	59	249	-15	+1.1	+0.1	27	2.8	29	28	4
tAq	τ Aquarids	98	342	-12	+1.0	+0.4	63	2.5	96	30	3
uPh	υ Phoenicids	105	21	-43	+1.0	+0.5	48	3.0	47	17	2
oCy	o Cygnids	116	305	+47	+0.6	+0.2	37	2.7	72	98	8
Cap	Capricornids	126	305	-9	+0.9	+0.3	25	2.0	1654	1441	16
dAN	δ Aquarids North	139	339	-5	+1.0	+0.2	42	3.3	214	178	5
PAu	Pisces Australids	123	337	-33	+1.0	+0.4	42	3.2	412	241	5
dAZ	δ Aquarids South	125	339	-17	+0.8	+0.2	43	3.3	3460	601	11
iAZ	ι Aquarids South	135	338	-14	+1.0	+0.3	36	3.3	260	229	5
Per	Perseids	139	46	+58	+1.3	+0.1	61	2.5	14635	1201	10
kCy	κ Cygnids	145	289	+52	+0.6	+0.3	27	2.2	582	664	10
eEr	π Eridanids	154	52	-15	+0.8	+0.3	59	2.8	136	71	5
gDo	γDoradids	157	61	-50	+0.5	+0.2	41	2.8	67	34	5
Aur	Aurigids	158	72	43	+1.0	+0.2	69	2.7	28	37	4
kAq	κ Aquarids	176	338	-5	+0.9	+0.4	19	2.8	29	27	3
Eps	ϵ Geminids	206	103	+28	+0.7	+0.1	71	3.0	163	198	15
Ori	Orionids	208	95	+16	+0.7	+0.1	67	3.1	2428	417	16
LMi	Leo Minorids	211	162	+37	+1.0	-0.4	61	2.7	20	18	3
Tau	Taurids	220	48	+18[1]	+0.3	+0.1	30	2.3	2580	1275	16
dEr	δ Eridanids	230	55	-2	+0.9	+0.2	31	2.8	62	142	5
zPu	ζ Puppids	231	117	-42	+0.7	-0.2	41	3.4	215	83	3
Leo	Leonids	234	153	+22	+1.0	+0.4	71	3.4	160	181	13
PuV	Puppids/Velids	260	135	-46	+0.8	-0.4	40	2.9	706	263	5
Pho	Phoenicids	252	18	-58	+0.8	+0.4	18	2.8	77	122	6
Mon	Monocerotids	261	100	+14	+1.0	-0.1	43	3.5	110	145	9
Gem	Geminids	261	112	+32	+1.0	+0.1	36	*2.6	9692	450	16
sHy	σ Hydrusids	259	127	+2	+0.9	-0.3	59	3.0	307	148	10
Urs	Ursids	270	223	+78	-0.2	-0.3	35	3.4	237	132	9

Table 3b. Results from exponential curves fitted to the ZHR data of the main peak. Subsequent columns list the peak position ($\lambda_{\odot}^{max}$), the peak rate (ZHR_{max}), the slope of ascending and descending branches (B), average orbital elements, the mass of a zero magnitude meteor M(0), and the density of matter in the peak of the meteoroid stream (ρ; in g/cm^3). M_{1yr} is the mass in a flux tube of length 1 yr$\times V_H$, while M_{tot} is this mass multiplied by the mean period of the meteoroids. Values of M_{tot} between brackets are for an assumed period P = 20 yr (these streams lack photographically determined orbits). Note: *) orbital period of parent comet

Name	$\lambda_{\odot}^{max}$ (1950.0)	ZHR_{max}	B $^o)^{-1}$	P (yr)	q (AU)	i ^{o})	π ^{o})	M(0) (g)	ρ ($\times 10^{-24}$)	M_{1yr} ($\times 10^{14} g$)	M_{tot} ($\times 10^{15}$ g)
Boo	282.62±0.03	133±16	1.8(4)	5.3	0.98	72	94	0.51	19±3	0.29±0.05	0.15±0.03
gVe	285.0±1.0	2.4±0.4	0.12±0.03	2.7	0.91	56	138	1.13	0.42±0.07	1.0±0.4	0.27±0.10
aCu	(294.7)	(3.0±0.8)	(0.11±0.03)	∞	0.90	87	78	0.28	0.11±0.02	0.5±0.2	(1.0)
aHy	(299)	<2	-	19	0.31	56	221	0.46	<0.16	< 1.0	< 2
aCa	310.5±0.7	2.3±0.6	0.16±0.03	∞	0.97	37	144	4.18	3.1±0.8	1.8±0.6	(3.6)
dVe	(317)	<1.3	-	∞	0.90	49	182	1.13	<0.23	<5	< 10
aCe	318.7±0.5	7.3±1.5	0.18±0.03	∞	0.99	106	136	0.17	0.49±0.10	0.70±0.10	(1.4)
oCe	322.7±0.4	2.2±0.3	0.15±0.02	∞	0.87	86	187	0.26	0.090±0.012	0.20±0.03	(0.4)
tCe	(333)	<4.5	-	∞	0.90	128	180	0.14	<0.13	<4	-
dLe	334±3	1.1±0.3	0.049±0.015	2.73	0.61	5	237	5.79	1.4±0.4	2.1±0.6	0.56±0.18
Vir	(339)	<1.5	-	3.9	0.58	4	254	3.60	<1.06	<2.6	<1.0
gNo	352.3±0.5	5.8±1.0	0.19±0.03	∞	0.89	133	213	0.18	0.33±0.05	0.44±0.07	(0.89)
dPa	370.4±1.5	5.3±0.7	0.075±0.015	164*	0.94	107	163	0.14	0.15±0.02	1.2±0.3	20±6
Lyr	31.7±0.3	12.8±0.7	0.22± 0.01	329	0.92	80	246	0.31	0.72±0.04	0.77±0.03	25.2±0.9
mVi	39±2	2.2±0.5	0.045± 0.008	3.4	0.39	8	333	2.06	0.79±0.17	2.4±0.3	0.8±0.2
eAq	45.8±0.5	36.7± 5.0	0.080±0.014	11.2	0.58	166	141	0.10	0.56±0.09	1.8±0.4	2.0±0.5
CAu	(55)	<3.0	-	(1.4)	0.16	87	10	0.43	<0.15	<0.20	<0.03
Sco	55.2±0.9	3.2±0.4	0.13±0.03	3.65	0.24	6	355	1.13	1.04±0.13	1.4±0.5	0.5±0.2
oSc	71.9±0.4	5.2±1.4	0.15±0.04	3.86	0.73	3	321	8.25	10±3	3.6±1.2	1.4±0.5
Ari	76±1	54±12	0.10±0.03	2.3	0.09	28	108	0.82	9±4	36±15	8±3
Sag	88.5±1.1	2.4±0.5	0.037±0.005	4.3	0.42	4	7	2.35	1.11±0.23	3.7±0.3	1.6±0.2
Cet	95.0±0.7	3.6±1.1	0.18±0.04	∞	0.93	143	244	0.096	0.08±0.03	0.060±0.007	(0.12)
Oph	(97)	(2.3)	(0.037)	2.8	0.39	3	6	3.10	(1.6)	(4.8)	(1.3)
tAq	97.3±0.5	7.1±1.6	0.24±0.05	∞	0.44	176	13	0.11	0.20±0.05	0.12±0.02	(0.24)
uPh	110.5±0.5	5.0±1.9	0.25±0.05	∞	0.96	82	321	0.33	0.20±0.08	0.16±0.02	(0.32)
oCy	116.0±0.5	2.5±0.8	0.13±0.03	∞	0.90	56	339	0.91	0.49±0.15	1.06±0.15	(2.1)
Cap	121.7±0.9	2.2±0.3	0.041±0.007	3.8	0.59	7	37	4.19	5.6±0.7	12±3	4.6±0.8
dAN	123.4±1.0	1.0±0.2	0.063±0.020	4.2	0.07	20	111	0.56	0.055±0.011	0.6±0.2	0.25±0.11
PAu	123.7±0.7	(2.9±0.8)	(0.26±0.05)	9.0	0.17	45	57	0.56	(0.18±0.05)	(0.11±0.04)	(0.10±0.04)
dAZ	124.9±0.3	11.4±1.2	0.091±0.010	5.4	0.10	26	99	0.51	0.56±0.07	3.0±0.4	1.6±0.2
iAZ	131.0±1.0	1.5±0.3	0.070±0.015	3.6	0.25	4	76	1.01	0.18±0.04	0.47±0.13	0.17±0.02
Per	139.49±0.04	84±5	0.20±0.01	135	0.92	113	289	0.13	2.73±0.18	2.92±0.12	39.5±1.5
kCy	146.0±0.8	2.3±0.4	0.069±0.005	9.5	1.04	38	348	3.10	3.3±0.6	13.5±0.3	12.8±0.5
eEr	(152)	<40	-	∞	0.41	81	107	0.15	<0.9	<2	-
gDo	155.0±0.5	4.8±1.6	0.18±0.06	∞	0.97	64	3	0.61	0.52±0.12	0.7±0.2	(1.4)
Aur	(157.5±0.5)	(9±3)	0.19±0.04	49	0.95	149	312	0.08	0.11±0.04	0.04±0.02	0.19±0.08
kAq	176.5±0.8	2.7± 0.5	0.11±0.04	5.7	0.83	2	54	12.2	9.5±1.8	2.9±1.3	1.7±1.1
Eps	206.0±1.0	2.9±0.6	0.082±0.008	133	0.78	173	90	0.07	0.019±0.004	0.0049±0.0009	0.066±0.015
Ori	207.9±0.4	25±4	0.12±0.02	39	0.58	164	111	0.09	0.18±0.04	0.27±0.09	1.1±0.3
LMi	209.0±0.7	1.9±0.7	0.14±0.05	449	0.65	124	317	0.13	0.04±0.02	0.09±0.03	4.1±1.5
Tau	222.9±1.0	7.3±1.0	0.026±0.003	3.3	0.39	5	154	2.06	6.0±0.8	31±3	10.3±1.1
dEr	(228)	< 0.9	-	∞	0.50	21	140	1.81	<0.4	<0.4	-
zPu	231.5±0.5	3.2±0.4	0.13±0.03	∞	0.96	89	5	0.61	0.18±0.02	0.47±0.16	(0.93)
Leo	234.4±0.3	23±6	0.39±0.08	54	0.98	162	48	0.07	0.084±0.023	0.0012±0.0002	0.007±0.001
PuV	251±1	4.5±0.7	0.034±0.006	1.8	0.97	70	78	0.67	0.48±0.07	16±3	3.0±0.6
Pho	251.7±0.5	2.8±0.8	0.30±0.16	5.1	0.92	12	74	15.0	13±3	0.7±0.5	0.4±0.3
Mon	260.2±0.6	2.0±0.4	0.25±0.10	534	0.18	37	209	0.51	0.084±0.014	0.06±0.02	3.3±1.0
Gem	261.4±0.1	88±4	0.39(4)/0.72(10)	1.68	0.14	24	225	1.01	22.1±1.1	3.3±0.6	0.55±0.11
sHy	264.8±0.8	2.5±0.5	0.10±0.03	37	0.25	127	199	0.15	0.039±0.009	0.17±0.04	0.6±0.2
Urs	270.3±0.3	(11.8±2.5)	(0.61±0.12)	14	0.95	53	116	1.13	1.5±0.3	0.13±0.04	0.19±0.08

Table 3c. Some streams are best represented by a sum of two exponential curves as in Eq. 8: a main peak (p) and a background (b). Values are given of peak activity ZHR_{max}, slopes of rising (B^+) and decending (B^-) branches, and total mass estimates M_{tot} of the two components.

Name	$\lambda_\odot^{max}$	ZHR_{max}^p	B^p	M_{tot}^p	ZHR_{max}^b	B^{b+}	B^{b-}	M_{tot}^b	M^b/M^p	M_{tot}
Boo	282.62	110±20	2.5±0.5	0.06±0.02	20±4	0.37±0.10	~0.45	0.41±0.16	7±4	0.5±0.2
Pau	123.7	2.0±0.5	~ 0.40	~0.03	0.9±0.1	0.03±0.01	~0.10	0.25±0.11	8±6	0.3±0.2
Per	139.44	70±5	0.35±0.03	10.7±1.2	23±2	0.050±0.005	0.092±0.009	35±5	3.1±0.4	46±5
Leo	234.4	19±6	0.55±0.15	0.0027±0.0011	4±1	0.025±0.006	>0.15	0.021±0.007	8±4	0.024±0.007
Gem	261.4	74±4	(0.59/0.81)±0.07	0.23±0.03	18±2	0.09±0.03	0.31±0.12	1.2±0.5	5±2	1.4±0.5
Urs	270.3	10±3	0.9±0.4	0.07±0.04	2.0±0.5	0.08±0.03	0.2±0.1	0.5±0.4	7±6	0.6±0.5

A circular cross section is assumed, based on the observation that the median cross section of streams (0.08 AU) is similar to the "rule of thumb" distance between comet orbit and Earth's orbit to give an observable stream. For wide streams with inclination less than 15 degrees, a value of B = 0.19 is taken perpendicular to the ecliptic plane. The same value is adopted for wide background components. The strong asymmetry in the background of, for example, the Perseids suggests that dust in the background component is less wide spread perpendicular to the stream than in the Earth's path.

6.2. Results

Results are presented in Table 3b. Error estimates describe the certainty of the fit of Eq. 8 to the data points only and does not include possible systematic errors. The mass estimates are in good agreement with recent estimates by Hughes (1990) and Stohl (1986). Table 4 summarizes a number of estimates found in the literature. The estimates of some of the major streams vary by as much as three orders of magnitude. Part of this discrepancy is due to uncertainties related to the shape of the activity profile, which are constrained in this study.

6.3. Discussion

Other uncertainties remain. The total mass estimate is affected by the uncertainty in the detection probability (i.e. effective surface area, sampling efficiency, etc.), the uncertainty in the median period of the meteoroids, an unknown stream width perpendicular to the path of the Earth, uncertainties in the behaviour of χ with magnitude (and mass range over which is integrated), and an uncertain magnitude versus mass relationship.

The detection probability function P(m) may affect the absolute rates systematically by about 50% (Appendix). Uncertainties in the period vary widely (from 10% up to a factor of 10, if any information is available at all) and can be judged from the photographic surveys of orbital elements. This uncertainty can only be diminished by future surveys. Errors due to a non-circular cross section can be as much as a factor of 10, although usually should not exceed a factor of three or so. Perhaps, future model calculations will allow accurate estimates of the 2-d cross section of streams. Conversion to a non-circular cross section is straightforward. It is also possible to converse the mass estimates by adopting another relationship of mass and magnitude. If visual light is emitted proportional to kinetic energy, then $M \sim 10^{-0.4m}$, instead of $M \sim 10^{-0.62m}$. This causes the mass estimates to differ by up to a factor of 10 for $\chi = 3.5$, but much less for smaller χ. In this case, the mass is dominated by small grains for $\chi > 2.51$. The uncertainty in the mass of a zero magnitude meteor is probably about a factor 2. Perhaps, these relationships can be established with more certainty in the future. Finally, the mass estimates can be improved (by a factor of 2 - 4?) if more information becomes available on the size distribution (or χ) for small and large masses.

Table 4. Comparison of total mass estimates with similar estimates found in the literature. All values are in units of 10^{15} g

stream	this study	comparison	reference
Gem	1.4	5.7	Lovell 1954
		2.0	Hughes 1974
		0.04	McCrosky 1975
		16	Hughes & McBride 1989
		1.6	Hughes 1990
Per	46	2.0	Lovell 1954
		0.88	Hughes 1974
		2	Hughes & McBride 1989
		31	Hughes 1990
Boo	0.5	0.5	Lovell 1954
		0.046	Hughes 1974
		1.3	Hughes & McBride 1989
		0.13	Hughes 1990
Ori	1.1	50	McIntosh & Hajduk 1983
		0.21	Jones 1983
		3.3	Hughes & McBride 1989
		7	McIntosh 1990 influx by Jones
		200	McIntosh 1990 influx by Hajduk
Tau	10.3	16	Stohl 1986

7. Summary and conclusions

Meteor counts performed by the 16 dedicated amateur astronomers listed in Table 1 have resulted in a homogeneous set of meteor stream activity profiles.

All major streams are well represented by exponential increasing and decreasing slopes in activity, resulting in straight lines in a log–normal plot. There is no evidence for stable submaxima in the stream profiles. The main peak of most streams

is symmetric. Exceptions are the Geminids and Bootids, which also are the narrowest streams (with the possible exception of the Ursids). These streams are exceptional too because of a strong variation of χ with solar longitude.

In a few cases there is a significant background component, in first order well represented by exponential slopes. The background component is asymmetric, in all cases with a more shallow component in the rising branch. The well observed rising branch in the background of the Perseids suggests a shoulder near $\lambda_{\odot}$=130.

I assume that all minor streams are represented by a similar (single) set of exponential curves and proceed to calculate slopes (B) and peak activity values (ZHR_{max}) (Table 3b). These values, when inserted in Eq. 8, can be compared to future observations.

Typical short period meteoroid streams have a slope of B$\sim$0.19 (Eq. 8), which corresponds to an equivalent cross section of 0.08 AU. This is similar to the typical distance between comet orbit and Earth orbit needed to give a detectable stream, which suggests that the stream cross section is usually fairly circular. Wide streams are found mainly among orbits with inclination less than 15 degrees and small perihelion distance (with the exception of PuV, kCy, and dPa). These streams are likely extended in the plane of the ecliptic more than in the direction perpendicular to the path of the Earth and the ecliptic plane.

Estimates of the total mass in each stream are given in Table 3b. The current mass estimates are for an assumed circular cross section (except as indicated), a mass regime between 10^{-6} and 10^{2} g, and M(m) according to Jacchia et al. (1967). Uncertainties in these parameters cause the final mass estimates to be uncertain by typically an order of magnitude. But conversion to a non-circular cross section, a different mass regime, or a different relationship between mass and magnitude is straightforward.

It is hoped that meteor counts are continued in the future in order to monitor the position and strength of maximum activity of the major streams and to gain statistical weight for the minor streams.

Acknowledgements. This work heavily weighs on the exemplary effort by Jeff Wood and Rudolf Veltman in stimulating visual observers to continue observing for many consecutive years, gathering the data, and publishing acounts of single returns. Jeff Wood prepared clear and detailed reports of the NAPO-MS visual observations and continued doing so for many years. In a similar persistent effort, Hans Betlem edited the visual reports of DMS and published the journal Radiant. The data were processed at Leiden Observatory. Maarten Wiertz assisted in entering the data into a database. The author was motivated to write the paper due to enjoyable observing nights with Rudolf Veltman and many fruitful discussions with members of the DMS, notably Paul van der Veen, Marc de Lignie, Casper ter Kuile, Klaas Jobse, Koen Miskotte, Annemarie Zoete, Hildo Mostert, Carl Johannink, Michiel van Vliet, and Marco Langbroek, as well as with members of other amateur organisations amongst whom are Juergen Rendtel, George Spalding, and Masahiro Koseki. Jeff Wood provided information on the observing procedures of the NAPO-MS. Many more observers than the 16 selected for this study are active in both the North-Australian Planetary Observers Meteor-Section and the Dutch Meteor Society, each of whom contributed invaluably to the continuity of the observations.

Appendix A: mass estimates

A.1. Influx rate

The distribution of particle masses in a meteoroid stream is assumed to be continuous and according to a power law, resulting in a meteor distribution: (e.g. Kresakova 1966):

$$n(m) = n(0)\,\chi^{m} \tag{10}$$

where χ is the magnitude distribution index. χ is assumed to be constant over a range in magnitude (m), for example between -3 and +5 magn.

Only a fraction N(m) of all incident meteors n(m) is recorded by a standard visual observer. The probability function P(m) is defined such that (Kresakova 1966):

$$N(m) = n(0)\,P(m)\,\chi^{m} \tag{11}$$

The Zenith Hourly Rate is the sum of all observed meteors per unit time:

$$ZHR = n(0) \sum_{m} P(m)\chi^{m} \tag{12}$$

If χ and P(m) are known, n(0) can be derived from the ZHR.

The observed rate of magnitude zero meteors n(0) is somewhat less than the true number of incident magnitude zero meteors, because of the effect of variable extinction and distance to the observer. The correction from apparent to absolute (= at 100 km distance) magnitude for individual meteors (Δm) is (Porubcan & Zvolankova 1984):

$$sin(h) = \frac{H}{2R}[\frac{2R}{H} + 1 - 10^{0.4\Delta m}]10^{-0.2\Delta m} \tag{13}$$

where an extinction coefficient of k = 0.4 is adopted. h is the altitude of the meteor above the horizon, H is its height above the Earth surface, R the diameter of the Earth. With H$\sim$95 km and R = 6366 km, this correction amounts to 0.5 magnitudes at h = 54° and 1.5 magn at h = 32°. Consider altitudes of h > 32° only. Meteors of a mass typical of magnitude zero meteors in the zenith that appear above h = 54° (40% of that part of the sky) are seen as such, while those between 54° and 32° are classified as magnitude +1 meteors. The correction becomes:

$$n(0) \Leftarrow n(0)(0.4 + 0.6\chi) \tag{14}$$

The next step is to normalise n(0) to unit area and time. The effective surface area (A_E) considered here, i.e. h> 32°, depends on the height where meteors reach their maximum brightness, which depends on the entry velocity. For heights between 70 km (V_{∞} = 20 km/s) and 100 km (V_{∞} = 72 km/s), A_E ranges from 3.84×10^{14} to $7.74 \times 10^{14} cm^2$. The rate of magnitude zero meteors in the peak of the stream is:

$$n(0) = \frac{ZHR_{max}(0.4 + 0.6\chi)}{(\sum_m P(m)\chi^m)\,A_E\,3600} \tag{15}$$

The total mass influx is (from Eq. 10):

$$F_M = n(0) \sum_m M(m)\, \chi^m \tag{16}$$

where the mass of a meteor M of magnitude m is given by (Jacchia et al. 1967) from Super Schmidt photography:

$$logM(g) = 5.15 - 0.44 m_{ph}(magn.) - 3.89 log V_\infty (km/s)$$
$$-0.67 log(sin(h_r)) \tag{17}$$

Photographic magnitudes relate to visual magnitude estimates as: $m_v = 0.71\ m_{ph} + 1.30$ over the interval for which these relations are derived ($-0.5 < m_v < 2.5$). Therefore, Eq. 17 equals:

$$logM(g) = 6.06 - 0.62 m_v - 3.89 log V_\infty \quad (-0.5 < m_v < 2) \tag{18}$$

where the small $sin(h_r)$-term is neglected, by adopting a reasonable $h_r = 45^o$. The mass of a zero magnitude meteor is:

$$M(0) = 10^{6.06 - 3.89 log(V_\infty)} \tag{19}$$

and the influx rate becomes:

$$F_M = n(0)\, M(0) \sum_m 10^{(log\chi - 0.62)m} \tag{20}$$

where V_∞ is in km/s. The summation is over the magnitude interval where χ is assumed constant. Note that for all $log\chi - 0.62 < 0$, i.e. $\chi < 4.17$, the total mass is dominated by large grains.

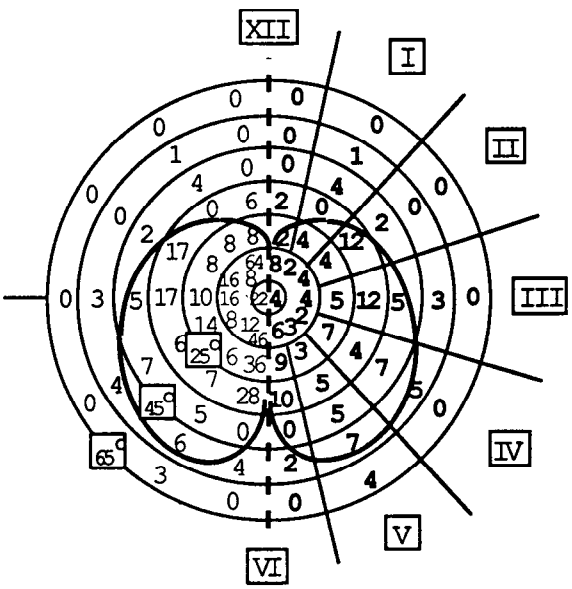

Fig. 13. The vertical asymmetry in the meteor detection probability. The field of view has a butterfly shape. The graph shows, as a function of the distance from center of vision and hour angle (up = 12 hours, etc.), the number of Geminids (right: absolute number; left: per unit area on the sky) as observed by the author from a location in the South of France during the night Dec. 13/14, 1990, between 00:00 and 03:00 UTC. The center of vision was on the radiant and close to the zenith

A.2. The probability function

I have derived the probability function P(m) for a standard observer from a series of DCV (Distance from Center of Vision) estimates by observers Jobse, Veltman, and Jenniskens using the method described by (Jenniskens 1989c). The observations are done at standard limiting magnitude Lm = 6.5 and the usual observing conditions regarding obstruction, viewing direction, etc. The method assumes that all +2 and brighter meteors are seen in an area with diameter 15° around the center of vision. The number of weaker meteors seen in this area is corrected by adopting a value of χ derived from the brighter meteor distribution (m < +2). Then a homogeneous distribution of meteors is assumed for the whole sky with $h > 32^o$. The actually observed number relative to the calculated total number gives P(m).

The result for two typical observing conditions is summarized in Table 5. +52N refers to conditions in the Netherlands, where the limiting magnitude often tends to drop quickly toward the horizon. +44N refers to conditions with transparent skies down to the horizon as during observations in the South of France. Our observers, accustomed to conditions in the Netherlands, tend to miss more faint meteors near the center of vision but notice more bright meteors farther out when observing in perfect transparent skies. The relevant parameter is $\sum_m P(m)\chi^m$, which, of course, is χ dependent. Values for χ = 2.5 and χ = 3.5 are listed in Table 5 and compared to literature data. I find values a factor of 2 less than those of Kresakova (1966) and observer Rendtel ($c_p = 1.3 \pm 0.2$) in Koschack & Rendtel (1990b).

Figure 13 is illustrative of how detection sensitivity falls off for D > 15°. A loss of meteors in the central area would cause an overestimation of $\Sigma_m P(m)\chi^m$, opposite to what is suggested. On the other hand, P(m) values wil be a factor 1.8 larger if the DCV limit of 15° is actually at 20° for all three observers. Such systematic error may occur due to the intrinsic length of meteors. A compromise between P(m) from DCV estimates and those of Kresakova (1966) and Koschack & Rendtel (1990b) probably is the best estimate for P(m) of a standard observer (Table 5, adopted).

A.3. Mass density and mass

The density of matter in the peak of the meteoroid stream (in g/cm^3) is given by:

$$\rho = \frac{F_M}{10^5 V_G} \tag{21}$$

with V_G the geocentric velocity of the meteoroids (in km/s):

$$V_G = \sqrt{V_\infty^2 - 11.2^2} \tag{22}$$

The total influx of matter perpendicular to V_G has to be transformed into one perpendicular to the heliocentric velocity of the meteoroids (V_H). The velocity of the meteoroids in their orbit at a distance R_E from the Sun is:

$$V_H = V_E \sqrt{2/R_E - 1/a} \tag{23}$$

Table 5. Probability function of a standard observer, for an observing surface at altitudes above $h > 32°$, from a location in the Netherlands (+52N) and the South of France (+44N). Conditions in the Netherlands include horizon obstruction and a fast drop of limiting magnitude to lower altitudes. The results are compared to data from [1] Kresakova (1966) and [2] observer J. Rendtel in Koschack & Rendtel (1990b)

m_v	P(m) +52N	P(m) +44N	P(m) [1]	P(m) [2]	adopted
-2	0.58	0.72	0.75	0.99	0.75
-1	0.44	0.72	0.73	0.99	0.73
0	0.36	0.72	0.70	0.99	0.70
1	0.26	0.58	0.68	0.80	0.63
2	0.19	0.33	0.64	0.64	0.48
3	0.14	0.21	0.43	0.35	0.32
4	0.072	0.046	0.12	0.10	0.09
5	0.016	0.0051	0.015	0.030	0.009
6	0.002	-.-	0.00013	0.007	0.001
$\Sigma_m P\, 2.5^m$	9.5	10.2	20	22	15
$\Sigma_m P\, 3.5^m$	33	26	56	71	43

from which V_H is obtained by inserting $R_E = R_\oplus = 1$ AU in good approximation (a in AU). The angle δ between V_G and the heliocentric velocity vector of the Earth ($V_E \sim 29 - 30$ km/s) is obtained from:

$$sin(\delta) = \frac{1}{V_G}\sqrt{V_H^2 - (\frac{V_H^2 - V_G^2 + V_E^2}{2V_E})^2} \quad (24)$$

Define the equivalent cross section (Δ t) along the Earth's path from:

$$\Delta t * ZHR_{max} = \int_{-\infty}^{\lambda_{\odot max}} ZHR^+ d\lambda_\odot + \int_{\lambda_{\odot max}}^{\infty} ZHR^- d\lambda_\odot \quad (25)$$

where ZHR^+ and ZHR^- refer to the ascending and descending branches of the ZHR curve. For the general shape of the ZHR curve in Eq. 8, the equivalent cross section is (in units of degree solar longitude):

$$\Delta t = (\frac{1}{B_+} + \frac{1}{B_-})\frac{1}{ln(10)} \quad (26)$$

Perpendicular to the heliocentric velocity (V_H) of the meteors, the effective surface area becomes (Δt in seconds):

$$A = \pi \frac{\Delta t \Delta t_2}{4} (V_E (V_G/V_H) sin(\delta))^2 \quad (27)$$

where I allow a different equivalent cross section perpendicular to the Earth orbit (Δt_2). I assume $\Delta t_2 = 4.6$ degrees (B = 0.19) for streams with inclination less than 15 degrees and $\Delta t > 4.6°$, while $\Delta t_2 = \Delta t$ otherwise. Now the total mass, integrated over the whole flux tube, i.e. multiplied by the period of the particles P, is given by:

$$M_{tot} = 2.43 \times 10^{27} F_M \pi \frac{\Delta t_1 \Delta t_2}{4} V_E^2 (V_G/V_H) sin^2\delta P \quad (28)$$

with Δt in degrees, P in yr, and V_E in km/s. Table 3b lists values of M_{tot} as well as values of the total mass given that P = 1 yr (M_{1yr}).

References

Andreev G.V., Rubtsov L.N., Tarasova I.I., 1989, WGN 17, 249
Babadzhanov P.B., Kramer E.N., 1965, Smits. Contr. to Astrophys. 11, 67
Bel'kovich O.I., Sulejmanov N.I., Tokhtas'ev V.S., 1984, BAC 35, 123
Cevolani G., Hadjuk A., 1987, in *Interplanetary Matter*, Publ. no. 67 of the Astron. Inst. Czech. Acad. Sci., Z. Ceplecha, P. Pechina (eds.), p 179
Bone N., 1993, *Meteors*, Sky Publishing Co., Cambridge (Ms).
Cook A.F., 1973, in *Evolutionary and Physical Properties of Meteoroids*, NASA-SP 319, Washington D.C., 183
Denning W.F., 1898, Astron. Nachr. 148, 283 (nr. 3546)
Drummond J.D., 1981, ICARUS 47, 500
Ellyett C.D., 1977, J. Geophys. Res. 82, 1455
Fox K.A., Hughes D.W., Williams I.P., 1982, MNRAS 200, 313
Gatrell G., Elford W.G., 1975, Austr. J. Phys. 28, 591
Grygar J., Kohoutek L., 1965, BAC 16, 273
Hajduk A, 1980, in *Solid Particles in the solar system*, I. Halliday, B.A. McIntosh (eds.), p. 149
Hajduk A., 1986, ESA-SP 250 vol 2., p. 239
Hindley K.B., 1971, J. Brit. astron. Assoc. 82, 57
Hughes D.W., 1974, Nature 252, 191
Hughes D.W., 1976, in *Space Research XVI*, Berlin 1976, 333
Hughes D.W., 1978, in *Cosmic Dust*, J.A.M. McDonnell (ed.), p. 123
Hughes D.W., Williams I.P., Murray C.D., 1979, MNRAS 189, 493
Hughes D.W., Williams I.P., Fox K.,1981, MNRAS 195, 625
Hughes D.W., 1982, Vistas in Astronomy 26, 325
Hughes D.W., 1982a, The Observatory, 102, 42
Hugehs D.W., McBride N., 1989, MNRAS 240, 73
Hughes D.W., 1990, MNRAS 245, 198
Jacchia L.G., Whipple F.L., 1961, Smits. Contr. to Astrophys. 4, 97
Jacchia L.G., Verniani F., Briggs R.E., 1967, Smits. Contr. to Astrophys. 10, 25
Jenniskens P., 1986, Radiant 8, 120
Jenniskens P., 1988, DMS Visueel Handboek (Dutch Meteor Society, Leiden)
Jenniskens P., 1989a, Radiant 11, 26
Jenniskens P., 1989b, Radiant 11, 123
Jenniskens P., 1989c, Radiant Letters 1, 3
Jenniskens P., 1991, Radiant 13, 126
Jenniskens P., Wiertz M., de Lignie M., 1991 Radiant 13. 20
Jenniskens P., 1992a, Radiant 14, 28
Jenniskens P., 1992b, Radiant 14, 55
Jenniskens P., 1994, *Meteor stream activity. 2. Meteor outbursts* A& A submited
Jones J., 1983, MNRAS 204, 765
Jones J., 1985, MNRAS 217, 523
Kaiser T.R., Poole L.M.G., Webster A.R.. 1966, MNRAS 132, 225
Knöfel A, 1990, WGN 18, 61
Koschack R., Rendtel J., 1990a, WGN 18, 44
Koschack R., Rendtel J., 1990b, WGN 18, 119
Koschack R., 1991, WGN 19, 225
Kresák L., 1964, BAC 15, 53
Kresák L., Porubçan V., 1970, BAC 21, 153
Kresáková M., 1966, Contr. Astr. Obs. Skalnaté Pleso 3, 75

ter Kuile C., 1989, Radiant 11, 101
Levin B.J., 1955, in *Meteors*, Supplement (Vol. 2) to J. Atmosph. Terr. Phys. , 131
Lindblad B.A., 1968, IAU Symp. 33, Kresak & Millman (eds.), p. 50
Lindblad B.A., 1971, Smiths. Contr. to Astroph. 12, 1
Lindblad B.A., 1978, Nature 273, 732
Lindblad B.A., 1980, in *Solid Particles in the Solar System*, I. Halliday & B.A. McIntosh (eds.), 105
Lindblad B.A., Simek M., 1986, ACM II, C.I. Lagerkvist et al. (eds.), 537
Lovell A.C.B., 1954, *Meteor Astronomy*, Oxford Clarendon Press
Marsden B.G., 1983, *Catalogue of Cometary Orbits*
Mason J.W., Sharp I.D., 1981, J. BAA 93, 4
McCrosky R.E., Posen A., 1961, Smits. Cont. to Astrophys. 4, 15
McCrosky R.E., 1975, in *The Dusty Universe*, Smits. Astrophys. Obs., p. 169
McIntosh B.A., Simek M., 1980, BAC 31, 39
McIntosh B.A., Hajduk A., 1983, MNRAS 205, 931
McIntosh B.A., Simek M., 1984, BAC 35, 14
McIntosh B.A., Jones J., 1988, MNRAS 235, 673
McIntosh B.A., 1990, in *Comet Halley - Investigations, results, interpretations*, ed. John Mason, Vol 2, 121
McIntosh B.A., 1991, in *Comets in the Post Halley Era*, R.L. Newburn, M. Neugebauer, J. Rahe (eds), 567
Millman P.M., 1967, Smiths. Contr. to Astroph. 11, 151
Murray C.D., Hughes D.W., Williams I.P., 1980, MNRAS 190. 733
Nolle M., Koch B., 1988, Radiant 10, 4
Nilsson C.S., 1964, Aust. J. Phys. 17, 205
Olsson-Steel D., 1987, Austr. J. of Astron. 2, 21
Opik E.J., 1940, Tartu Obs. Publ. 30, 33
Opik E.J., 1958, Armagh Obs. Contr. 26, 47
Poole L.M.G., Hughes D.W., Kaiser T.R., 1972, MNRAS 156, 223
Porubcan V., Zvolankova J., 1984, Contr. Astr. Obs. Skalnaté Pleso 12, 279
Porubcan V., 1986, ACM II, C. Lagerkvist et al. (eds.), 527
Porubcan V., Hajduk A., McIntosh B., 1991, BAC 42, 199
Prentice J.P.M., 1953, J. Brit. Astron. Assoc. 63, 175
Rendtel J., 1990a, *IMO working list of meteor showers*
Rendtel J., 1990b, WGN 18, 81
Rendtel J., Alt R., Brown P., 1993a, WGN 21, 19
Rendtel J., Koschack R., Alt R., 1993b, WGN 21, 97
Roggemans P., 1987, WGN 15, 181
Roggemans P., 1989 WGN 17, 127
Roggemans P., Koschack R., 1991, WGN 19, 184
Simek M., 1975, BAC 26, 1
Simek M., 1978, BAC 29, 331
Simek M., 1987a, BAC 38, 1
Simek M., 1987b, BAC 38, 80
Simek M., Lindblad B.A., 1990, ACM III, C.-I. Lagerkvist et al. (eds.), 567
Simek M., McIntosh B.A., 1986, BAC 37, 146
Shepherd J., 1978, Meteoros 9, 2
Spalding G.H., 1982, J. Brit. Astron. Assoc. 92, 227
Spalding G.H., 1984, J. Brit. Astron. Assoc. 94, 109
Spalding G.H., 1987, J. Brit. Astron. Assoc. 98, 26
Srirama Rao M., Raja Ratman S., Jagan Mohana Rao J.V.R., 1978, Indian Journal of Radio- and Space Physics 7, 229
Stohl J., Porubcan V., 1978, Contr. Astr. Obs. Skalnaté Pleso 10, 39
Stohl J., 1986 in *20th ESLAB Symp. on the Expl. of Halley's Comet*, ESA-SP 250 Vol 2., 27
Van der Veen P., 1986a, Radiant 8, 1
Van der Veen P., 1986b, Radiant 8, 41
Van der Veen P., 1989, Radiant 11, 32
Veltman R., 1983a, Radiant 5, 61
Veltman R., 1983b, Radiant 5, 111
Veltman R., 1984, Radiant 6, 20
Veltman R., 1985, Radiant 7, 79
Veltman R., 1986a, Radiant 8, 34
Veltman R., 1986b, Radiant 8, 62
Webster A.R., Kaiser T.R., Poole L.M.G., 1966, MNRAS 133, 309
Whipple F.L., 1951, ApJ 113, 464
Williams I.P., Murray C.D., Hughes D.W., 1979, MNRAS 189, 483
Wood J.C., 1981, Radiant 3, 39
Wood J.C., 1982a, W.A.M.S. Bulletin nr. 110
Wood J.C., 1982b, W.A.M.S. Bulletin nr. 175
Wood J.C., 1986, N.A.P.O.-M.S. Bulletin nr. 1
Znojil V., Hollan J., Hajduk A., 1987, BAC 38, 372
Zvolankova J., 1983, BAC 34, 122
Zvolankova J., 1984, Contr. Astr. Obs. Skalnaté Pleso 12, 45

This article was processed by the author using Springer-Verlag TEX A&A macro package 1992.